IONIC MOBILITY AND SUPERPLASTICITY IN CERAMICS

by

Anne L. Vilette

Thesis submitted to the faculty of the
Virginia Polytechnic Institute and State University
in partial fulfillment of the requirements for the degree of

MASTER OF SCIENCE

in

Materials Science and Engineering

APPROVED:

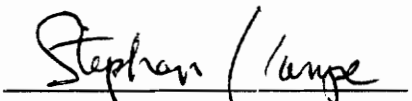

S.L. Kampe, chair

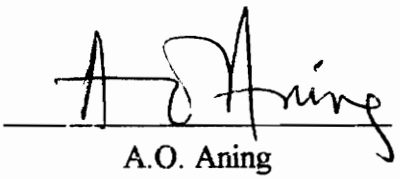

A.O. Aning

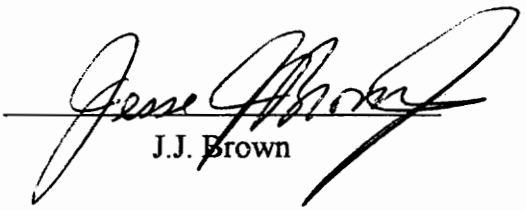

J.J. Brown

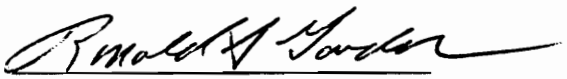

R.S. Gordon

September, 1994

Blacksburg, Virginia

.2

IONIC MOBILITY AND SUPERPLASTICITY IN CERAMICS

By

Anne L. Vilette

Committee Chairman: Stephen L. Kampe
Materials Science and Engineering

(ABSTRACT)

Superplasticity and superionic conductivity (SIC), both thermally activated processes, have been independently observed in certain materials with a high diffusion coefficient in high temperature ranges. Intuitively, this observation leads one to the idea that both types of behavior may be inter-related with one another. Therefore, it is the purpose of this research to investigate, specifically, the deformation characteristics of two SIC's, Bi_2O_3 and YSZ (yttria-stabilized zirconia), and to attempt a correlation of their behavior. Compressive deformation of these two materials was conducted over a wide range of temperatures and at various strain rates in an effort to characterize the temperature and/or strain-rate dependences of any observed superplasticity. Steady-state flow stress values were utilized to calculate the strain-rate sensitivity, m, of the materials, as well as the activation energies (Q_c) of superplasticity. Next, the obtained values of Q_c were compared to SIC activation energies from the literature.

Bi_2O_3 exhibited structural superplasticity within the range of test conditions utilized. However, published values of SIC activation energy were lower than experimentally derived Q_c by a factor of four. Therefore, one is not able to state whether or not there is any correlation between the two behaviors. Unfortunately, YSZ exhibited brittle behavior over the entire temperature and strain-rate ranges, so the same analysis could not be performed. Furthermore, SEM micrographs showed that YSZ samples, as processed, did not possess the proper microstructure required for superplasticity. Hence, no final conclusions on YSZ can be drawn from this study.

ACKNOWLEGMENTS

The author wishes to acknowledge her advisor, Dr. S.L. Kampe, for his directions and his support and Drs. A.O. Aning, J.J. Brown, R.S. Gordon and D. Hirschfeld for their time and interest. Also the author would like to thank the Center for Advanced Ceramic Materials (CACM) for its support.

Special thanks are due to the graduate students of the Materials Science and Engineering department who were very patient, especially to Dilip Vijay and Bill Russ who were extremely helpful, and to Mike Stawovy and Dave Teter who were very entertaining.

The author would like to express her gratitude to Dr. J.R. Mahan, coordinator of the exchange program between Virginia Tech. and the Université de Technologie de Compiègne, France, that permitted her to enroll in the Master's program of the Materials Science and Engineering Department.

The author also wants to thank all her friends who made this American experience so enjoyable. Special thanks to the "French Connection": Anne-Claire, Benoît and Eric, without whom the French club would not have been "Frenchship", and to the "American" Friends": Bob, Jim, Kermit, and Robert.

Finally, the author would like to thank her grand-parents, Roberte and Gaston, for their encouragement and support throughout her studies. This thesis is dedicated to them.

TABLE OF CONTENTS

LIST OF FIGURES

LIST OF TABLES

1. INTRODUCTION

The ability of a material to undergo superplastic deformation offers significant opportunities for cost-effective manufacturing, especially for components which combine complex geometry and large sizes. The manufacturing advantage is particularly notable in instances where a material may be difficult to fabricate by conventional means. An example of the successful utilization of superplastic deformation as a viable manufacturing method is exemplified by the production of various manifolds, ducts, frames, structural geometries, and pans for the aerospace and medical industries fabricated from various high strength titanium-based metallic alloys [1].

Though evidence has been available for several years, it has just been recognized that certain ceramic materials are capable of exhibiting superplastic behavior. This behavior suggests an alternative means to manufacture traditionally difficult-to-fabricate ceramic components. Indeed, the successful extension of superplastic forming as a manufacturing technique to ceramic materials creates the potential for an economically viable method of creating ceramics for numerous automotive, aerospace, and hypersonic applications.

Because the recognition of superplasticity in ceramics is relatively new, a unified theory or prediction of superplastic deformation in ceramics does not currently exist. Similarly absent are guidelines or correlations to predict such behavior based on certain fundamental material properties.

The present work represents initial efforts towards examining potential correlations between the ability of a ceramic to be superplastically formed with a fundamental material property, namely the material's ionic conductivity. The materials which have been shown to exhibit superplasticity may also exhibit exceptional solid state conductivities, the latter

of a magnitude on the order of those expected for a liquid. Such behavior is known as super-ionic conductivity.

2. LITERATURE BACKGROUND

2.1. SUPERPLASTICITY

2.1.1. GENERAL

The term "superplasticity", which is derived from the Latin prefix "super" meaning excess and the Greek word "plastikos" meaning to give form [2], first appeared in 1959 in the paper by Lozinsky and Simeonova [3], titled "Superplasticity of commercial iron under cyclic fluctuations of temperature". This term characterizes the ability of certain materials to undergo extensive uniform plastic deformations that can reach thousands percent (often without the formation of a neck in tensile testing) prior to failure at elevated temperatures. Although this property is essentially observed in polycrystalline solids, it is interesting that hot glass represents the ideal superplastic material with a strain rate sensitivity of unity and a potential for virtually infinite deformation in either tension or compression [2].

Superplasticity can be classified primarily into two phenomenological-based categories:

- temperature cycling or internal stress superplasticity
- structural superplasticity.

The first kind of superplasticity, which is also the less studied, was first brought to the fore in 1924 by Sauveur [4]. He observed an "anomalous" deformation of a considerable magnitude during a phase transition (α to γ) in a Fe sample. This type of behavior was termed "amorphous plasticity" by Koref [5] in 1926 when he studied enhanced plasticity of tungsten coils during recrystallization.

However, extensive studies on this kind of deformation started only in 1959 following the work of Jong and Ratheneau [6] and their development of quantitative relationships between stress and strain during thermal cycling of iron. Nevertheless, most of these studies were performed on metallic solids. The first proof of this kind of superplasticity in ceramics was first made by Johnson et al. in 1975 [7]. They observed an elongation of 115% in Bi_2O_3 sample at 730°C during the transition from the monoclinic to the cubic phase.

The second type of superplastic behavior, structural superplasticity, which is related to the microstructure of the material and obtained at a constant temperature, is thought to have been recently discovered. Indeed, the phenomenon was first described by Bengough [8] in 1912 in a paper which dealt with an $\alpha+\beta$ brass that showed an elongation of 163% at 700°C. Nevertheless, there is a distinct possibility that some materials used in ancient times and having the same structural properties observed later in superplastic samples, could have been superplastic. The ancient arsenic bronzes (Cu-As) containing up to 10 weight per cent of As and used in early Bronze Period, i.e., around 2500 BC, in Turkey, and the ancient steel of Damascus (1.6-1.9% C Steel) in use from 300 BC to the late 19th century are two typical examples [9].

Following Bengough's paper, the main publication in this field was by Pearson [10] who detailed an elongation of 1950% in an aged Bi-44% Sn eutectic alloy. As a result of this exemplary observation, illustrated in Fig. 2.1, Pearson's article is often credited for the first investigation on this subject.

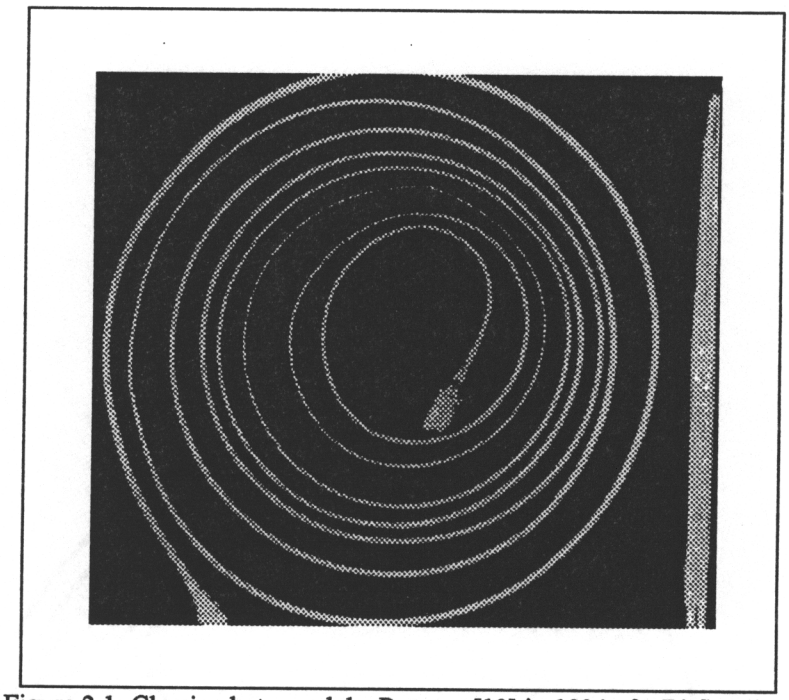

Figure 2.1: Classic photograph by Pearson [10] in 1934 of a Bi-Sn alloy.

Nevertheless, it was only after 1962 that the real interest in structural superplasticity appeared with Underwood's report [11] of an elongation of 650% at 250°C for a 20% Al and 80% Zn alloy that was quenched from a relatively low temperature (375°C). Furthermore, in 1964, Backofen [12] formed a superplastic Zn-Al alloy in an hemispherical shape by a simple air pressure forming operation as shown in Fig. 2.2.

As a result of the two successful investigations, a commercial infatuation was created based on:

- the ability to form superplastic materials in complex shapes easily because of their low resistance to plastic flow and their high plasticity.

- the economical considerations, i.e., the needs for expensive machining and joining operations were obviated.

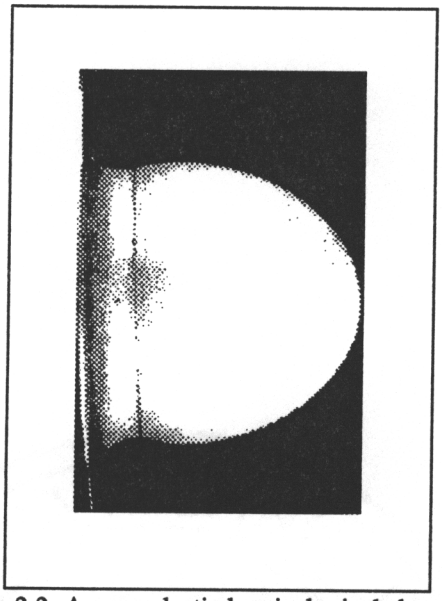

Figure 2.2: A superplastic hemispherical shape of a Zn-Al alloy from Backofen et al in 1964 [12].

Consequently, there was a stronger driving force for understanding superplastic behavior. However most of the research was done on metals in the establishment of the principles of structural superplasticity and are hence relatively well understood. By comparison, the investigations on the other kinds of materials such as ceramics or intermetallic alloys were not so numerous and essentially started in the 1980's. In particular, the superplastic behavior in ceramics was first proved by Wakai and co-workers [13] in 1986 in their study on yttria-stabilized tetragonal zirconia polycrystals (Y-TZP) that exhibited an elongation of 120% at a constant temperature of 1723K.

2.1.2. PRINCIPLES

In the previous section, superplasticity was distinguished into temperature-cycling superplasticity and structural superplasticity. The first kind of behavior, also known as internal stress superplasticity, relates to the enhanced ductility generated by internal

stresses induced by thermal cycling. Furthermore this appellation includes two different phenomena:

- The first one, of minor importance, is due to internal stresses instigated by temperature cycling in a polycrystalline material having anisotropic thermal expansion. For example, we can cite the case of a sample of uranium elongated to 300% under thermal cycling, whereas its maximum elongation obtained under constant temperature is around 50% [14]. However, this phenomenon has not been reported in the literature for ceramic materials.

- The second one is caused by internal stresses induced by a temperature cycling of a polymorphic material through a phase change. For example, we can cite the case of a sample of 52100 steel elongated to 700% under thermal cycling through an allotropic transformation and under a stress of 17 MPa [9]. Several mechanisms that are not universally accepted have been proposed to explain the large deformation occurring in metals under a small external stress. Lozinsky and Simeonova [3] expressed the idea of a momentary loss of coherency at the transition interface. Porter and Rosenthal [15] suggested that there exists a high susceptibility to deformation in the new, transformed, dislocation-free phase. Clinard and Sherby [16] explained the high deformation by diffusion of the excess point defects existing at he transformation interface. Greenwood and Johnson [17] estimated the permanent deformation activated by the internal stresses created at the transformation interface by the volume variation during the transition. Then, any kind of applied stress, however small, only tends to enhance the effect if internal stress causing a net macroscopic deformation that appears to originate from the applied stress. Nieh and McNally [18] suggested the generation of mobile dislocations induced by internal stresses created during the thermal cycling. Finally, Sherby and Wadsworth [9]

proposed an explanation more related to a strain hardening effect than to a strain rate sensitivity effect.

The second kind of superplasticity, structural superplasticity, can be defined as a large deformation under conditions of constant temperature without any phase transformation. Several requirements are necessary to obtain this kind of behavior [19]. In metals, these requirements are the following:

1. a stable uniform, equiaxed, ultra-fine microstructure. In general, the grain size has to be smaller than 10 μm.

2. a lack of intergranular brittleness, i.e., the grain boundaries need to be high-angled, mobile and must be resistant to tensile separation.

3. a high temperature ($T > 0.5\ T_{mp}$, where T_{mp} is the homologous melting point temperature of the material). This requirement is a direct consequence of superplasticity being a diffusion-controlled phenomenon.

The first and the last prerequisites are often difficult to obtain simultaneously. In general, there is an increase in the grain size with increasing temperature. This grain growth can be avoided or considerably restricted by the presence of a second phase as it is for:

- a two phase eutectic or eutectoid alloy (e.g., Zn-22%Al or Al-33%Cu)
- a matrix with particles incorporated (e.g., $ZrAl_3$ in Al-6%Cu-0.5%Zr) [14].

Both kinds of superplasticity represent a state of dynamic mechanical-microstructural equilibrium, as defined by an imposed rate of strain, microstructural recovery, and atomic mobilities of a magnitude capable of retaining microstructural volumetric continuity under the imposed strain rate. The requirement of atomic mobility can be partially alleviated if the grain size of the material is small. In fact, small grain size not only reduces the average

required diffusion distance, but also results in a higher fraction of grain boundary area and leads to an associated larger potential contribution from grain boundary diffusion. As a result, superplasticity is generally described by the following relationships:

$$\sigma = B\dot{\varepsilon}^m \tag{2.1}$$

where σ is the steady state flow stress

B is a constant related to the temperature and the microstructure

$\dot{\varepsilon}$ is the strain rate

and m is the strain rate sensitivity ($m = \frac{\delta \ln \sigma}{\delta \ln \dot{\varepsilon}}$).

Or, alternatively,

$$\dot{\varepsilon} = AD_0 \exp(-\frac{Q_c}{RT})(\frac{1}{d})^p \sigma^n \tag{2.2}$$

where $\dot{\varepsilon}$ is the steady state strain rate

A is a constant related to the structure of the material

D_0 is the diffusivity (diffusion preexponential constant)

Q_c is the activation energy for creep or superplasticity

R is the gas constant

T is the absolute temperature

d is the grain size

p is the grain size exponent

σ is the stress required to maintain the steady state strain rate

and n is the stress exponent (n = 1/m).

These equations delineate the general requirements for superplasticity, i.e., high diffusivities, low activation energy for high temperature deformation and fine grain size.

The general tendency for the stress versus strain rate behavior is shown in Fig. 2.3.

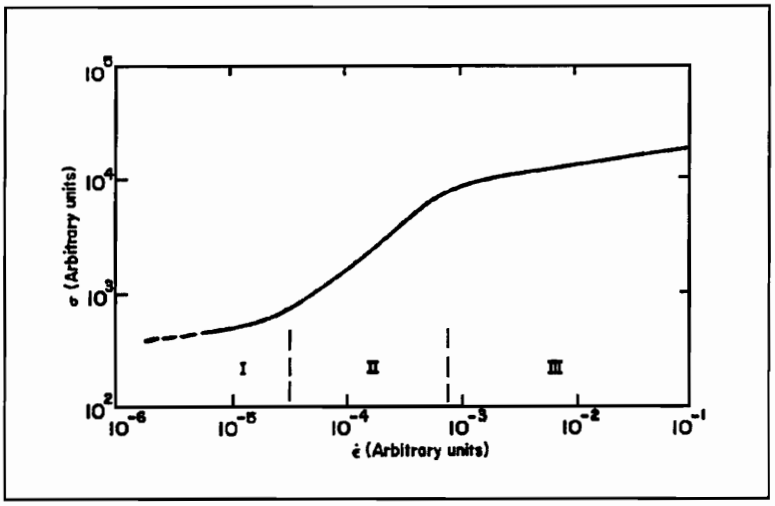

Figure 2.3: Schematic illustration of steady-state flow stress σ against strain rate $\dot{\varepsilon}$ for a superplastic metal [14].

It is obvious from this figure that three different regions exist. Region I, for which the value of the strain rate sensitivity, m, is low (about 0.2 in most of the cases), corresponds to the diffusion creep zone wherein an elongation of the grains occurs. Region II with a higher value of m ($0.2<m<0.5$) represents the superplastic zone corresponding to maximum contributions from grain boundary sliding, minimal grain elongation, and grain rotation. Finally, Region III, for which the value of m once again becomes low, corresponds to the traditional mechanism of deformation, i.e., the dislocation creep [2].

The values of the strain rate sensitivity, m, for which a superplastic behavior is observed are in the range of 0.3 to 1 [18,19]. For this range of m values, neck formation is difficult. Pilling and Norman [2] explained this effect to be the result of strain rate

hardening in the neck region. In a material subject to a tensile strain, the presence of a neck leads to a high strain-rate locally. If the value of m is high for the material, a sharp increase in the flow stress can occur within the necked region and this arrests any further development. As a result, a high value of the strain rate sensitivity is indicative of a high resistance to neck formation and thus a potential for high deformation. For this reason, materials with m values greater than approximately 0.3 are considered to be capable of superplasticity. The value of m also helps to define some of the mechanisms occurring during the deformation:

- When m is equal to one, the equation (2.1) corresponds to the equation used for the ideal Newtonian viscous fluids for which unlimited elongation is possible [20].

- When m is equal to 0.5, the mechanism proposed is the grain boundary sliding which is considered throughout the literature as the principal factor responsible for superplasticity. This mechanism is illustrated in Fig. 2.4a.

Another important mechanism that can occur in superplasticity is grain boundary sliding accompanied by grain boundary cavitation as illustrated on Fig. 2.4b. Cavitation along grain boundaries can lead to extensive grain sliding and rearrangement. However, the presence of cavities often limits the macroscopic value of ductility under tensile loading, hence masking the presence of this mechanism. Conversely, this mechanism is believed responsible for instances where the deformation and strain-rate sensitivity are very high in compression (where microscopic sensitivity to cavitation is negligible), but show limited ductility in tension.

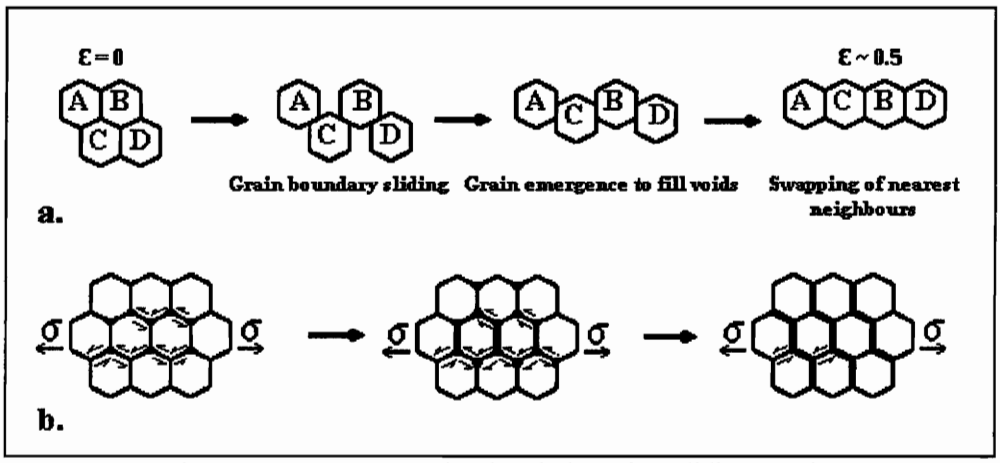

Figure 2.4: a) Unaccomodated grain boundary sliding [2]. b) Schematic model of grain boundary sliding accommodated by formation of cavities at triple junctions [24].

2.1.3. SUPERPLASTICITY IN CERAMICS.

Ceramic materials are known for their brittle character. While the general shape of the stress/strain curves for conventional metals are similar to that obtained for superplastic materials (though with less elongation), the shape of this kind of curve for most of ceramics is typically largely dissimilar, as shown in Fig. 2.5.

Furthermore, while ceramics can commonly exhibit fine grained microstructures (grain size < 10 μm) and good performance at high temperatures (e.g., high Young's modulus, high thermal resistance, etc.), their diffusivities and activation energies for atomic motion are often of a magnitude too great to ever expect that superplasticity was attainable. However, enhanced plasticity in certain ceramics, albeit less spectacular than in metals, was discovered 1967 [21]. The implications of this discovery are very important, i.e., superplasticity may represent a means to fabricate ceramics which were heretofore difficult due to the manufacturing difficulties attributed to their brittleness.

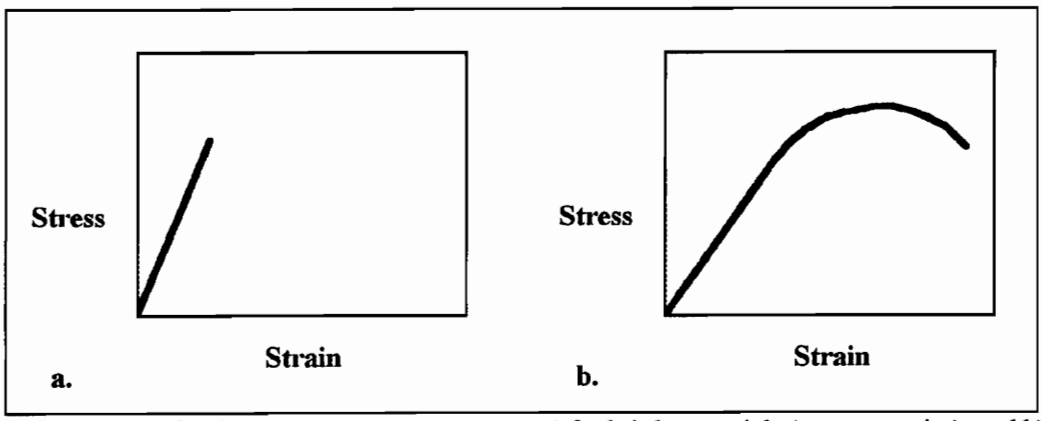

Figure 2.5: Stress - Strain curve at room temperature a) for brittle materials (most ceramics), and b) for ductile materials (most metals).

Since its discovery, the two types of superplasticity previously documented for metals have been reported for ceramics. However, fundamental understanding of the behavior is still in its infancy. Nonetheless, some attempts at the development of theory have been provided.

First, transformation superplasticity, defined as a large deformation which occurs in response to stresses generated during thermal cycling through a phase transition of a polymorphic material, has been observed in compressive tests and explained by different mechanisms.

The first theory was stated by Johnson et al. [7] in 1975 in their study on Bi_2O_3. Although "anomalous" deflections were observed in a three-point bending specimen of unstabilized ZrO_2 during the monoclinic to cubic transition even earlier (1967) [21], they were the first to prove that ceramic superplastic behavior was analogous to metal superplasticity. They determined the principal criteria necessary for ceramics to obtain high ductility via transformation superplasticity:

- a fine grain size (which is a common criterion for every type of superplasticity)

- a large volume change during the phase transformation

- a high transition temperature (if T_t is the transition temperature and T_{mp} the absolute melting temperature, then T_t / T_{mp} must be greater than 0.75).

Tests were conducted on samples of Bi_2O_3 that satisfied the criteria for the transformation from its monoclinic to its cubic form. The effects of the applied stress, grain size, and heating rate on the transformational strain were studied. From an analysis of these results, the following conclusions were drawn:

- The linear relationship between the transformational strain and the stress agreed with Greenwood and Johnson 's model [17]:

$$\varepsilon_{trans} = A(\frac{\sigma \frac{\Delta V}{V}}{S}) \qquad (2.3)$$

where ε_{trans} is the transformational strain per temperature cycle,

A is a constant,

$\Delta V/V$ is the volumetric change associated with the transformation ($\Delta V/V$ = 7% for Bi_2O_3),

σ is the average stress applied during the transition,

and S is a parameter indicating deformation by either yielding or creep of the weaker of the two phases.

- The grain size sensitivity and the time dependency (low heating rates permitted larger ε_{trans}) are related to the grain boundary sliding effect. No transformational strain was observed when the grain size was greater than 20 μm.

They obtained the same kind of results with samples of Bi_2WO_6. Nevertheless, no value of strain rate sensitivity or stress exponent confirming these hypotheses were given in these investigations.

The same theory was also supported by J.R. Smyth et al in their study of transformational superplasticity in the Bi_2O_3-Sm_2O_3 system. The highest deformations were obtained for eutectoid composition (4 mol% of Sm_2O_3) [22].

Another theory was proposed by P.C. Panda and R. Raj in 1985 [23] in a study on fine-grained $MgO\text{-}2Al_2O_3$ spinel. They obtained very high ductility (more than 60% of deformation) in a compressive test at a temperature close to the solvus and at low strain rates. The change in flow stress was measured as a function of grain size and it was found that the flow stress tended to increase with a decreasing grain size. This result was inconsistent with the model based on diffusional process, and therefore, a dislocation creep mechanism, characterized by the development of subgrain boundaries and defined by the following relationship, was proposed.

$$\dot{\varepsilon} = A\sigma^n \exp(-\frac{Q}{RT}) \qquad (2.4)$$

Where $\dot{\varepsilon}$ is the strain rate,

A is the pre exponential factor,

Q is the activation energy,

n is the stress exponent ($n = 2.1 \pm 0.4$ for this case or $m = 0.48$),

and σ is the flow stress.

The conclusion of their study was that the high ductility was the result of a dynamic recrystallization process.

While the documentation on transformation superplasticity is limited, structural superplasticity in ceramics has been the subject of numerous publications since the early 1980's. Initially, most of the tests were done in compression but, since Wakai et al. [13] showed the high tensile ductility of yttria stabilized tetragonal zirconia (Y-TZP) in 1986, more and more tests have been made in tension and several ceramic materials have been experimentally identified as being capable of exhibiting the same kind of behavior. Typical examples include some glass ceramics [14] and some non-oxide ceramics [24] such as Si_3N_4 / SiC composites and shown in Fig. 2.6.

Many investigations have centered on yttria stabilized tetragonal zirconia and zirconia composites [25-30]. T.G. Langdon [20] provides a review of the results obtained by the several investigators of this material and has attempted to provide a general theory on structural superplasticity in ceramics. He states that all the documented results generally suggest that a diffusion-controlled process, with or without grain boundary sliding, is responsible for the superplastic behavior in these materials. This mechanism can be described, as in metals, by the relation (2.2):

$$\dot{\varepsilon} = AD_0 \exp(-\frac{Q_c}{RT})(\frac{1}{d})^p \sigma^n \qquad (2.2)$$

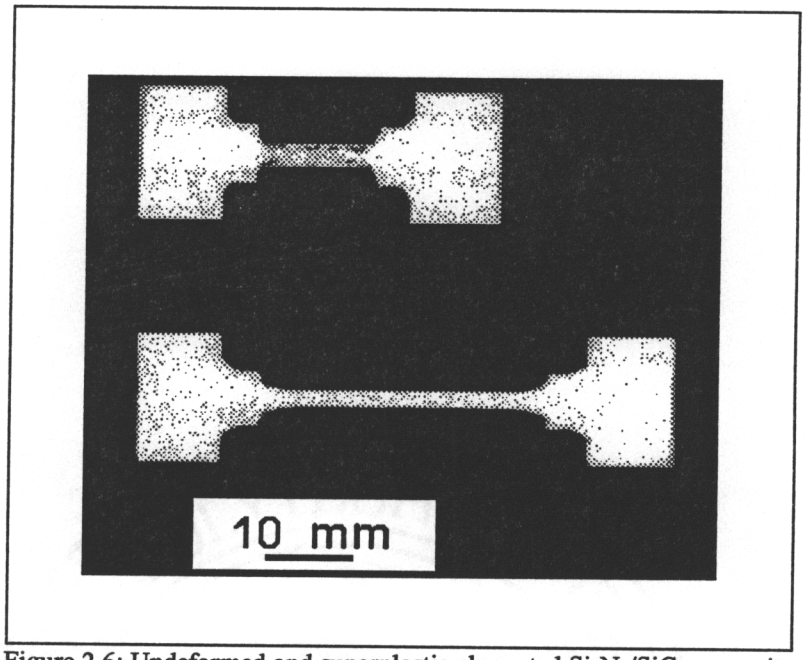

Figure 2.6: Undeformed and superplastic elongated Si_3N_4/SiC composite specimens [24].

However, whereas the mechanistic description of the deformation seems to be identical to that in metals, some differences exist:

1. The shape of the stress / strain rate curve is not similar. In metals, three regions are visible (Fig. 2.3) and, as a consequence, three different values of n ($n = 1 / m$, where m is the strain rate sensitivity) result. In ceramics, only one region is often observed. The value of m obtained in this region for ceramics is generally higher ($0.5 < m < 1$ for ceramics and $m \approx 0.5$ for metals) but is nonetheless still interpreted essentially to be indicative of grain boundary sliding.

2. The necessary grain size is smaller in superplastic ceramics (1 μm) than in superplastic metals (5 μm) [14].

3. In metals, the value of n is independent of the initial grain size, while this is not the case in ceramics, i.e., n tends to decrease as the initial grain size is increased.

4. There is no unique value of n for a ceramic material. The presence of impurities such as Al_2O_3 and SiO_2 can produce an intergranular glassy phase which can promote grain boundary mobility and influence the value of n [18]. n decreases when the area fraction of grain boundaries covered by the glassy phase increases [20]. The thickness Δ of this intergranular phase is related to grain size, d, [14] by:

$$\Delta = \frac{d}{2}(1-\frac{\sqrt{3}}{2}) \qquad (2.5)$$

Nevertheless, the value of Δ is reduced because of the non-uniform grain distribution, the grain deformation and the enhanced diffusion.

5. The value of the activation energy for stress flow, Q, decreases with increasing grain size.

In addition to the diffusion controlled process, mechanisms such as concurrent grain growth and concurrent grain boundary cavitation (in tensile tests) can also be present. Concurrent grain growth is often observed during superplastic deformations and is explained by A. Chokshi et al. [30] to be the result of the absence of any intergranular glassy phase.

2.2. IONIC CONDUCTIVITY AND SUPERIONIC CONDUCTIVITY

2.2.1. DEFINITIONS

2.2.1.1. IONIC CONDUCTIVITY

The application of an electric field on a conductor results in the generation of a current which can be described as the movement of electrons across the material. This phenomenon is characterized by the electrical conductivity σ:

$$\sigma = \frac{J}{E} \tag{2.6}$$

where E is the electric field strength,

and J is the electric-current density.

Conductivity can be classified into two types depending on the band gap of the material. If the size of the band gap is small, electrons can move from one atom to another through the lattice and electronic conductivity, σ_e, occurs. On the contrary, if the band gap is wide, electrons cannot be detached from the atoms. As a consequence, the current results from the movement of the charges along with the nuclei, which become the charge carriers, and ionic conductivity σ_i occurs. However, the two kinds of conductivity can also occur simultaneously and the total electric conductivity then represents their sum:

$$\sigma = \sigma_e + \sigma_i \tag{2.7}$$

The contribution of each type to the total conductivity is given by the transference number, t_X,

$$t_x = \frac{\sigma_x}{\sigma} \tag{2.8}$$

with $\sigma_x = \sigma_e$ or σ_i,

$$\text{and} \quad \sum_x t_x = t_e + t_i = 1. \tag{2.9}$$

For a perfect ionic conductor, the conductivity is totally ionic, $\sigma = \sigma_i$ and $t = t_i$.

In order to define more precisely ionic conductivity, some entities require further description. For example, in the expression for electrical conductivity (equation (2.6)), the current density, J, represents the charge crossing a unit of area in unit time and can be expressed as:

$$J = nqv \tag{2.10}$$

where n is the number of identical charge carriers

q is the charge on a carrier ($q = Ze$ where Z is the valence of the ion charge carrier and e the elemental charge of the electron, $e=1.6 \times 10^{-19}$ Coul) and v is the drift velocity of the carrier.

The current density can also be related to the mobility of the charge carriers, μ, since it is the proportionality factor between the drift velocity and the applied field, i.e.,

$$\mu = \frac{v}{E} \tag{2.11}$$

As a consequence from (2.10) and (2.11),

$$J = nq\mu E \tag{2.12}$$

And, from (6),

$$\sigma = nq\mu \tag{2.13}$$

The last relation is very useful in obtaining a general expression for ionic conductivity. The mobility of the ions carrying the charge can be related to their diffusion through the lattice by the Einstein relation:

$$\mu = \frac{q D_i(T)}{kT} \qquad (2.14)$$

where $D_i(T)$ is the diffusion coefficient of the charge carrier i at a temperature T,
k is the Boltzmann constant ($k = 1.38 \times 10^{-23}$ JK^{-1}),
and T is the absolute temperature in Kelvin.

Combining equations (13) and (14), we obtain the Nernst-Einstein prediction of ionic conductivity:

$$\sigma(T) = \frac{(Ze)^2}{kT} n(T) D(T) \qquad (2.15)$$

where n(T) is the number of charge carriers at a temperature T.

2.2.1.2. SUPERIONIC CONDUCTIVITY

Superionic conductivity occurs in certain materials as manifested by solid state conductivities of a magnitude typical of those found in molten salts. For example, whereas "normal" solid state conductivities are of the order of $10^{-8}(\Omega cm)^{-1}$ with a discontinuous change at the melting temperature, superionic conductivities are in the range of $1(\Omega cm)^{-1}$, a value typical of those found in ionic liquids [31]. Materials exhibiting such a behavior are called superionic conductors (SIC's), fast ion conductors (FIC's), or optimized ionic conductors. Fig 2.7 lists a few of the typical superionic conductors.

The expression (2.15) can also be used to describe the transport properties of the SIC's. However, the high speed ion transport and the large concentration of charge carriers in the

superionic conductors result in larger values of D(T) and n(T), respectively, 10^{-5} cm^2s^{-1} and 10^{22} carriers/cm3, than those found in regular ionic conductors.

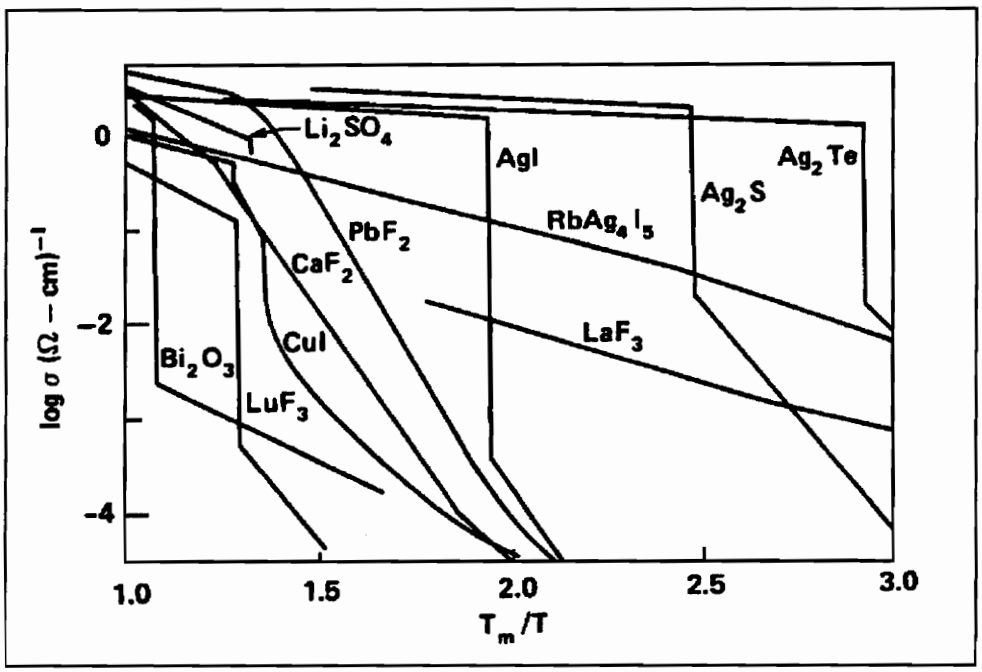

Figure 2.7: Conductivities of some typical superionics conductors plotted as a function of Tmp/T where Tmp is the melting temperature of the solid [31].

2.2.2. PRINCIPLES OF SUPERIONIC CONDUCTIVITY

Ionic conduction has been defined earlier as the movement of ions through the lattice. This kind of conduction is possible in superionic conductors via several structural features [32]. First, SIC structure consists of immobile and mobile ions arranged into two sublattices. At room temperature, both sublattices are ordered due to the low mobility of both kinds of ions. This order results in normal values of conductivity. At higher temperatures, often after a well-defined phase transformation, ionic conductivity is raised to exceptionally high values due to the disorder created within the mobile ion sublattice,

resulting in an increase of the ion mobility. The magnitude of conductivity is also the result of the thermal generation of point defects. As a consequence, while the immobile ions stay at fixed sites and do not contribute to the conduction, the mobile ions move between near-equivalent sites separated by continuous open channels of low activation energies (0.5 eV) [31,33]. These crystallographic sites are characterized by large voids present in the SIC structure and represent potential interstitial sites for the charge carriers [32]. Since their number is much larger than the number of mobile ions, empty sites are always available and charge carrier movement is, hence, always possible.

Superionic conductors has been classified in different ways. For example, Boyce [31] categorized them in three categories based on the transition to the high temperature superionic phase as illustrated in Fig. 2.8.

The first category represents the superionic conductors of type I characterized by a discontinuous change of the conductivity through a first order phase transition. In this kind of SIC, exemplified by AgI, Bi_2O_3 or ZrO_2, a rearrangement of the immobile ion sublattice occurs simultaneously with the disordering of the mobile ion sublattice at a fixed temperature.

For the second category, i.e., the SIC's of type II, the transition from the low conductivity at room temperature to the superionic conductivity is gradual and corresponds to a second order phase transformation. Additionally, there is no rearrangement of the immobile sublattice and the disordering of the second sublattice occurs progressively as the temperature increases. This is the case of PbF_2, CaF_2 and Na_2S, for example.

The last category, the SIC's of type III, are characterized by an exponential increase of their ionic conductivity with temperature and progresses without any apparent phase transition. The common examples of this kind of superionic conductivity, Na-β-Al_2O_3 and

$Li_2Ti_3O_7$, possess complex crystal structures and the mechanism involved is believed to be a kind of sublattice "melting".

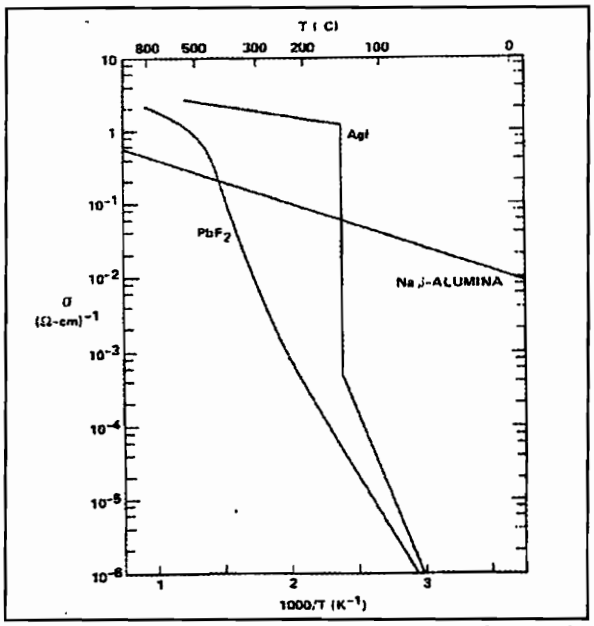

Figure 2.8: Conductivity vs. inverse of temperature for the three types of SIC's of Boyce's classification [31].

Hench and West [32] also differentiate three types of superionic conductors. The first group consists of halides and Chalcogenides of silver and copper with relative random bonding of the metal atoms. The second group is represented by oxides in the β-alumina structure and the third group by oxides in the fluorite structure.

The last classification has been developed by Tuller [33] and is related to the way by which the large number of charge carriers necessary for high ionic conduction, is reached. The first group, the "extrinsic conductors", consists of oxides in the fluorite structure, such as stabilized ZrO_2 and CeO_2, for which the conductivity increases with the addition of a dopant containing cations of lower valence than those present in the initial material. The contribution of the doping is to enhance the oxygen vacancy concentration and, as a

consequence, to increase the mobility of the charge carriers. The second group of superionic conductors, represented by α-AgI and δ-Bi_2O_3, is related to the high intrinsic disorder within the material: the large number of charge carriers are extremely mobile due to the fact the number of vacant sites is a lot greater. The characteristic of this kind of SIC's is that their conductivity is not enhanced by doping. Finally, for the third group, associated with polymer materials and also with intrinsic disorder, high value of conductivity is achieved by the formation of a disordered metastable phase.

2.2.3. APPLICATIONS OF SUPERIONIC CONDUCTORS

As discussed in the previous section, when an electric field is applied to a fast ionic conductor, there is a flow of charge resulting from the movement of ions (charge carriers). The result of this flow is a large conduction accompanied by a change in the composition of the material. Reversibly, if a gradient of chemical potential, i.e., a spatial distribution of concentration of mobile ions exists in the material, a flow of charge is induced and a current is created. This property accompanied by the high value of conductivity is utilized in a number of applications.

2.2.3.1. FUEL CELLS

A fuel cell is a result of the conversion of energy accompanying the diffusion of ions into electric power. As a consequence, it can be defined as an "energy-conversion system" [34]. Three generations of development of fuel cells can be differentiated depending on the type of electrolyte used: the earliest ones consisted of an aqueous solution of phosphoric acid as the electrolyte, the following ones contained melting carbonates and the recent ones are based on oxygen SIC's.

The third generation of fuel cells, also called Solid-State Oxygen Fuel Cells (SOFC) , consists of two chambers, filled with two different gases and separated by an oxygen SIC - most of the time Yttria- or Calcia-Stabilized Zirconia (YSZ or CSZ respectively). The SIC is covered on both sides by porous electrodes made of an electron-ion mixed conductor (Fig. 2.9). The role of the electrodes, which are often made of platinum, is to allow both ionic and electronic conduction so that the ionic current induced in the SIC can be converted into electronic current at the surface. To create this current, two different oxygen partial pressures, P'_{O_2} and P''_{O_2}, are imposed in the chambers on either side of the oxygen SIC heated to a temperature at which it is a conductor (1000°C for YSZ). For an ideal material of this kind, the electromotive force E (also called Nernst e.m.f.) is given by the following relationship:

$$E = \frac{kT}{4e} \ln(P'_{O_2} / P''_{O_2}) \qquad (2.16)$$

where e is the elemental charge of the electron.

This equation clearly indicates that a larger difference in the two partial pressures provides a higher e.m.f.. Consequently, the gases filling the two rooms have to be carefully chosen. In order to have an electromotive force in the range of 1V, one of the chamber needs to be occupied by pure oxygen and the other one by the fuel, a highly reducing gas such as hydrogen or methane [33].

The generation of electricity by fuel cells is an environmentally clean process. Indeed, when hydrogen is used as the reducing gas, the power generated induces a single chemical reaction between oxygen and hydrogen resulting in the production of only water.

Nevertheless, the SIC's used in this application have to fulfill several requirements. An obvious requirement is high ionic conductivity and low electronic conductivity.

Additionally, the SIC's need to possess high mechanical strength and high thermal shock resistance. Finally, they need to be chemically compatible with the electrodes.

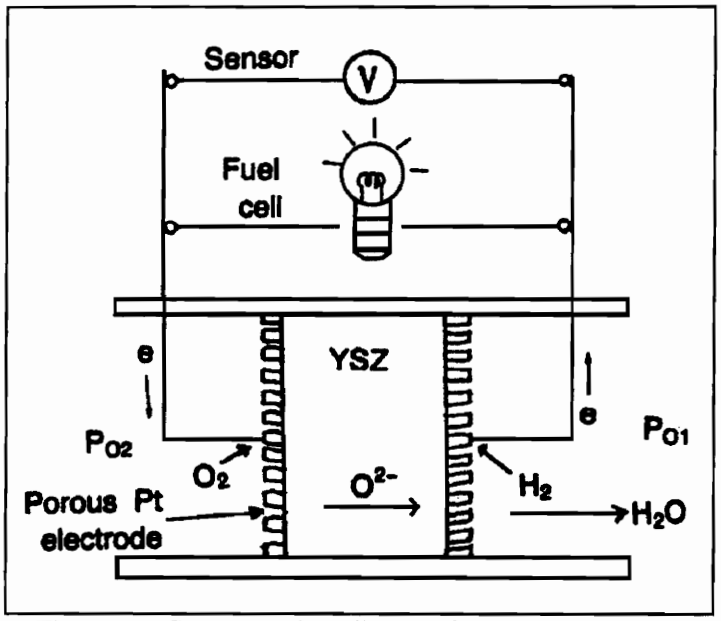

Figure 2.9: Concept of the solid-state fuel and sensors [34].

2.2.3.2. SENSORS

Gas sensors are essentially used as a mean to probe the waste gas of automobiles and characterize their content in an attempt to limit their emission of carbon monoxide and nitrous oxide [33]. Their principle of operation is the same as the one described in the last section for the fuel cells and are also illustrated by Fig. 2.9.

A superionic conductor (which is not necessarily an oxygen SIC) is coated with porous electrodes and surrounded by two gas chambers. However, only one of them is filled with a well characterized gas in terms of composition and pressure. The other chamber

contains the gas to be tested. If a difference of partial pressure of a particular gas consisting of the mobile ions of the SIC used exists between the two chambers, an electromotive force is created through the superionic conductor. The partial pressure of the gas can then be deduced using the Nernst equation (2.16).

2.2.3.3. BATTERIES

High energy batteries, extensively developped for power storage in electrical generating plants [33], are based on the principle of creation of high voltages by the combination of reactants with large free energy of reaction. They initially consisted of liquid electrolytes which are more and more substituted by chemicaly stable solid electrolytes in an effort to avoid problems of containment and stability. The solid electrolytes used in this application are cationic superionic conductors because of their ablility to achieve exceptionaly high conductivities at temperatures in the range of room temperature and 300°C.

2.2.3.4. OXYGEN IONIC PUMPS

Another utilization of oxygen superionic conductors is to regulate the oxygen concentration in oxide superconductors which are electron-ion mixed conducting materials [34]. In this kind of application, they act as oxygen ionic pumps with the following apparatus: the superconductor is covered on one side by an ion blocking electrode (Four-probe non-porous electrode) and on the other side by an oxygen superionic conductor coated on its free side by a porous electrode. When a dc current is applied from the non-porous electrode to the porous electrode, it generates a movement of the oxygen ions from the SIC to the superconductor which is stopped by the ion blocking electrode. As a consequence, the oxygen concentration of the material is increased. The process can be reversed by the inversion of the current direction and the change in concentration can be deduced from the Faraday equation:

$$M = \frac{It}{nF} \qquad (2.17)$$

where M is the number of mol of material transported,

I the intensity of the current,

t the duration of the process,

n the number of charges passed per atom,

and F the Faraday constant.

2.3. GUIDELINES OF THE RESEARCH

Since superplasticity and ionic conductivity have both been defined as thermally activated properties exhibited by some ceramic materials with a high diffusion coefficient, a possible relation between them seems conceivable.

To assess the potential correlations between superplasticity and superionic conductivity, it was necessary to first choose a material that had been documented to exhibit superplasticity and superionic conductivity. Samples of this material needed to be made and their superplastic deformability be confirmed by measuring the flow stress versus strain rate behavior over a range of temperatures. This could be done by noting the overall plastic deformation and by determining the strain-rate sensitivity constant, m, as a function of temperature.

The same procedure needed to be repeated with a material that had been documented to exhibit superionic conductivity, but no superplasticity.

3. PREPARATION OF THE SAMPLES.

3.1. CHOICE OF THE MATERIALS

In the previous chapter, superplasticity and superionic conductivity have been defined, along with the principal mechanisms responsible for the behavior. In addition, several ceramics exhibiting one or both of these properties have been mentioned. Tables I and II summarize the different ceramic materials that have been documented as exhibiting, individually, cited behaviors. Two compounds were chosen from these two tables. The first one needed to be both a superplastic and a superionic conductor. The only ceramic satisfying this demand was bismuth oxide (Bi_2O_3). Furthermore, a superionic material, not known for its superplasticity, was selected. An oxygen superionic conductor of type I was preferable for comparison of its mechanical properties with those of Bi_2O_3. This criterion led to yttria fully-stabilized zirconia (YSZ).

TABLE I: Examples of ceramics that have exhibited superplasticity [14].

Material	Type of superplasticity	Temperature (°C)	Strain %
Bi_2O_3	Transformation	730	-68
$MgO.2Al_2O_3$	Transformation	1550	-63
MgO	Structural	1327	> |-80|
Al_2O_3+0.05%MgO	Structural	1723	> |-39|
Al_2O_3+0.25%MgO	Structural	1693	> |-45|
Y-TZP	Structural	1723	> |-78|
Y-TZP+20%Al_2O_3	Structural	1772	> |-84|

TABLE II: Examples of superionic ceramic compounds [31].

Material	Behavior type	Mobile ion	$T_{transition}$ (°C)	T_{melt} (°C)
Li_2SO_4	I	Li	575	857
Bi_2O_3	I	O	730	824
Cu_2S	I	Cu	105 / 465	1127
YSZ	I	O	≈700	≈1700
PbF_2	II	F	430	822
Na_2O	II	Na	970	1130

3.1.1. BISMUTH OXIDE (Bi_2O_3).

Pure bismuth oxide or bismuth sesquioxide, Bi_2O_3, shows several crystallographic polymorphs [35]. The low temperature polymorph is the monoclinic phase, α, which is stable from room temperature up to 730°C. At a temperature of 730°C, it transforms to the fcc phase, δ-Bi_2O_3, and this transformation is accompanied by a large volume change. This second polymorph exhibits a high coefficient of thermal expansion and is stable up to the melting temperature (825°C). Nevertheless, two other metastable polymorphs can also be observed on cooling. The δ phase transforms to the α phase through one or two phase transformations that generate sudden volume changes causing cracks and deterioration in the mechanical properties of the material [36]. The intermediate phases involved are the tetragonal β-Bi_2O_3 formed at 650°C and the bcc γ-Bi_2O_3 formed at 639°C. The transition to the monoclinic structure occurs for both between 650 and 429°C. However, the γ phase can be quenched to room temperature [37].

The mechanical and electrical properties of Bi_2O_3 have both been characterized in the literature. For example, Johnson et al. [7] reported transformation superplasticity through

the monoclinic to cubic transition with the attainment of 0.68 of true strain. However, no investigation on structural superplasticity has ever been documented.

The bismuth oxide electrical properties have also been studied. Harwig and Gerards [37] characterized each of the polymorphs in terms of conductivity. Whereas the α phase is electronic (p type), the three other phases are predominantly ionic. Due to δ-Bi_2O_3's very high conductivity (approximately 1 $(\Omega cm)^{-1}$ and several orders of magnitude higher than β-Bi_2O_3 or γ-Bi_2O_3) resulting from its defect fluorite-type structure with 25% of the anion sites vacant, it has been the subject of many studies [33,36-41].

3.1.2. YTTRIA-STABILIZED ZIRCONIA (YSZ).

Pure zirconia, ZrO_2, also exhibits several crystallographic polymorphs [42]. The low temperature polymorph is the monoclinic phase which is stable from room temperature up to 1170°C. At a temperature of 1170°C, it transforms to the tetragonal phase and this transformation is accompanied by a large volume variation. The transition to the cubic phase which is stable up to the melting temperature, i.e., 2680°C, occurs at 2370°C.

The addition of oxides such as CaO and Y_2O_3 can modify the electrical and mechanical properties of the material. For example, yttria-partially stabilized zirconia with the addition of 3 mol% of Y_2O_3 has exhibited structural superplasticity [13,14,18-20,23-30]. The addition of higher concentration of yttria (7 mol% and up) lowers the transformation temperature of the cubic phase (Fig. 3.1) and increases of the oxygen ion vacancies at temperatures in the cubic structure leading to a high ionic conductivity (approximately 0.2 $(\Omega cm)^{-1}$) [43,44].

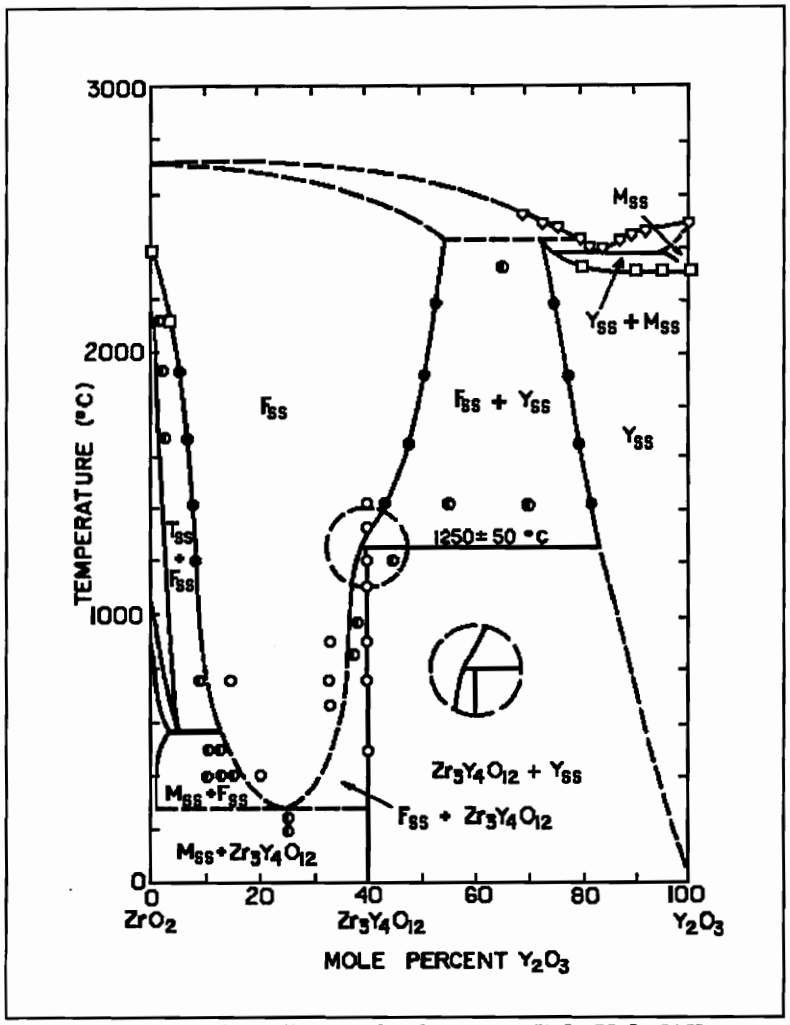

Figure 3.1: Phase diagram for the system ZrO_2-Y_2O_3 [45].

3.2. PROCESSING AND CHARACTERIZATION OF THE SAMPLES.

3.2.1. CHARACTERIZATION OF THE POWDER.

The powders of bismuth oxide (-30 mesh) and yttria-stabilized zirconia (ZrO_2+20wt% Y_2O_3) (-140mesh), obtained respectively from Cerac inc., Milwaukee, WI, and Atlantic Equipment Engineers, Bergenfield, NJ, were first observed under a Scanning Electron Microscope (SEM). The particle shapes of these powders were distinctly different from one another as shown in Figs. 3.2 and 3.3. Whereas Bi_2O_3 particles were irregularly shaped, stabilized zirconia were observed to be spherical.

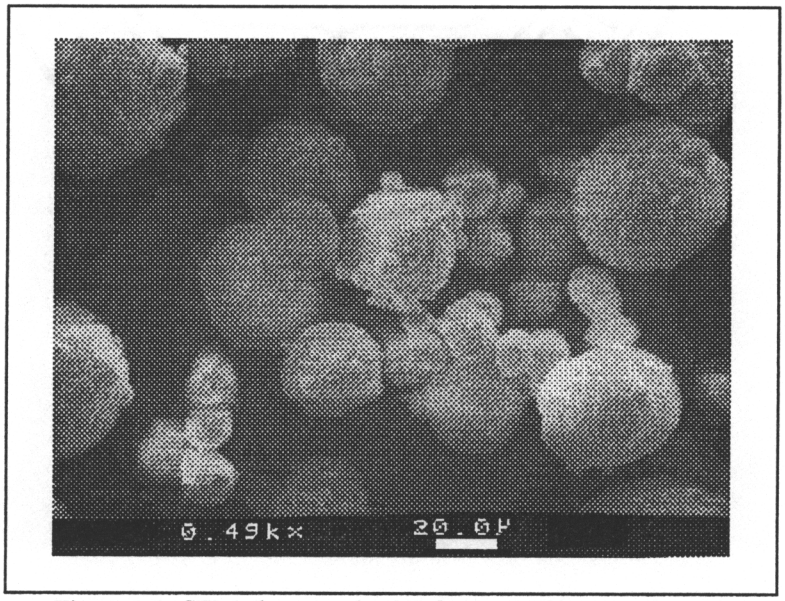

Figure 3.2: SEM photograph of ZrO_2 + 20wt% Y_2O_3 powder.

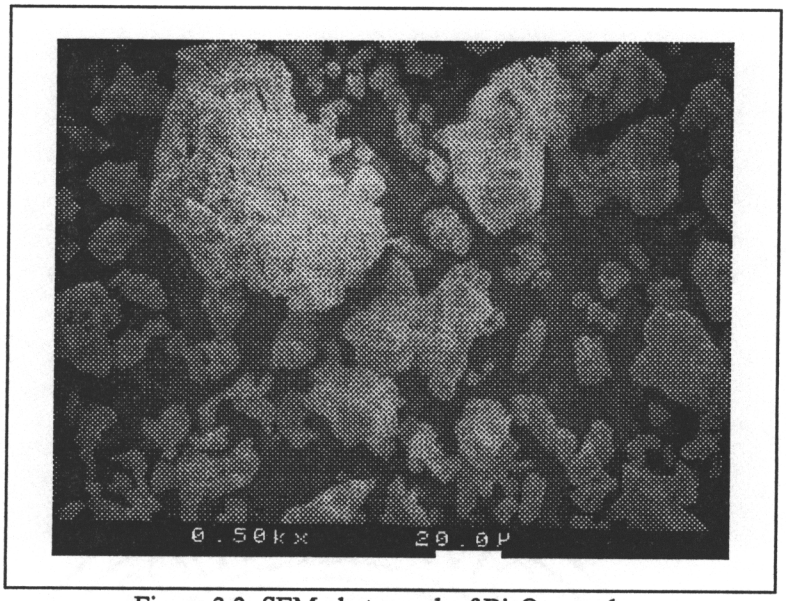

Figure 3.3: SEM photograph of Bi_2O_3 powder.

3.2.2. PRESSING OF THE SAMPLES.

3.2.2.1. THEORY OF COLD PRESSING AND SINTERING.

Cold pressing is a cost effective and simple ceramic-forming process. The powder is generally mixed with an organic binder and pressed in a metal die at pressures in the range of 3,000 to 30,000 psi. The densification process occurring during cold pressing has been described by Reed [46] as comprising of three steps. First, sliding and redistribution of the powder particles take place as they begin to deform or fracture under the applied pressure. As the pressure increases further, smaller and softer particles merge together and the largest porosity disappears. Finally, at high pressures, the large amount of the pores between the deformed and fractured particles is eliminated.

However, this process has some limitations, especially in terms of the length-to-diameter ratios of bodies that may be pressed. For example, if this ratio is too high, the

frictional forces generated during the pressing, especially those along the die wall, induce a pressure gradient within the piece resulting in an inhomogeneous density [47].

When the powder is pressed into the desired shape, the water and binder used to facilitate the pressing has to be removed by an operation known as **drying**. The ceramic body is heated to a temperature at which water and other additives to the powder can be evaporated (in the range of 100 to 300°C). This operation leads to a small amount of shrinkage resulting from the linking of the particles which were previously separated by water and other volatiles. Furthermore, this densification aids in preventing the material from cracking as it is heated to higher temperatures.

The last step in the process is **firing**. The pressed and dried powder is subsequently heated to a temperature at which atomic mobility, i.e., diffusion, is possible and grain growth accompanied by sintering occurs. As a result, density variation within the piece is virtually eliminated and porosity is decreased due to the flow of material as illustrated in Fig. 3.4. The temperature of firing is a function of the porosity, grain size, and density required by the particular application of the ceramic piece.

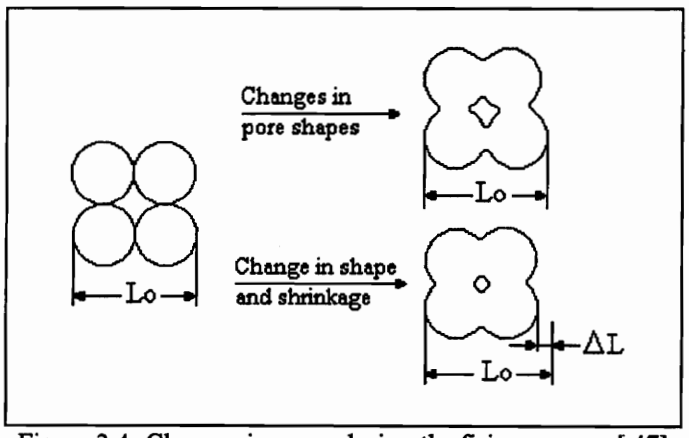

Figure 3.4: Changes in pores during the firing process [47]

3.2.2.2. EXPERIMENTAL PROCEDURE.

With a mortar and a pestle, 8 grams of Bi_2O_3 powder and 5 grams of stabilized-zirconia powder were milled separately with 3 wt% of Methocell, a cellulose ether binder, and a small quantity of water. They were then placed into a cylindrical die of 10 mm diameter. A pressure of 10,000 psi was applied to the upper part of the die and maintained for 3 minutes to compact the powder before being released. The pressed samples (∅10x15mm) were then placed into a furnace where they were dried and fired. Drying was done at 300°C (the temperature of evaporation of the binder) for two hours and then the samples were heated to the desired temperature of firing at a heating rate of 5°C/min. Different firing temperatures and times were tested so as to obtain samples with the highest density, lowest porosity, and the smallest grain size, which are some of the prerequisites for superplastic behavior.

For the bismuth oxide samples, the firing temperatures varied from 650°C to 800°C and firing times between 4 to 24 hours. The best compromise was obtained for a firing condition of 700°C for 24 hours, as illustrated in Fig. 3.5.

For the zirconia samples, firing conditions were varied from 1400°C to 1600°C for 3 to 9 hours and the optimum firing condition was determined to be 1600°C for 9 hours, as shown in Fig. 3.6.

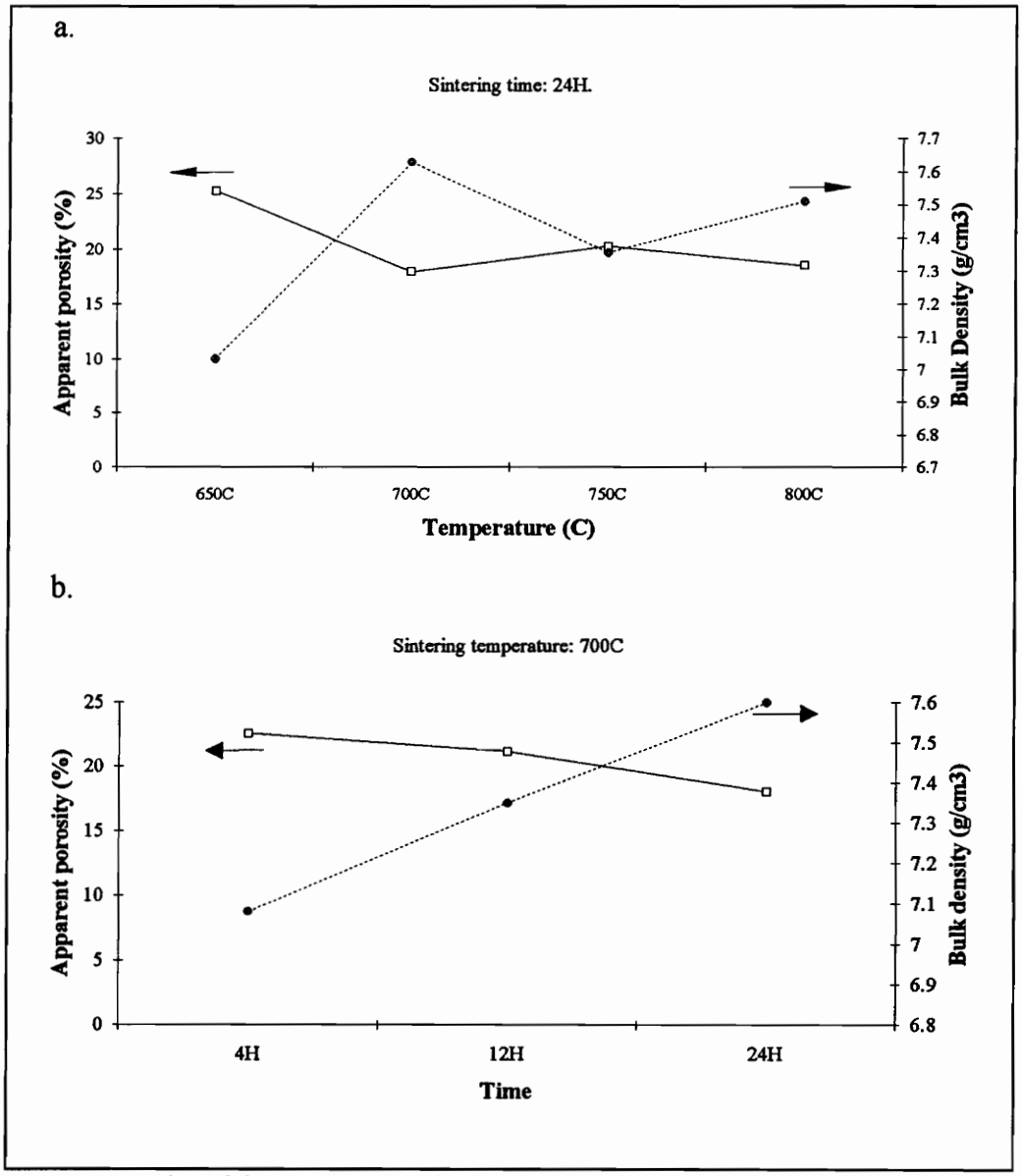

Figure 3.5: Variation of the apparent porosity and the bulk density of Bi_2O_3 samples as a function of a) the temperature of sintering, and b) the time of sintering

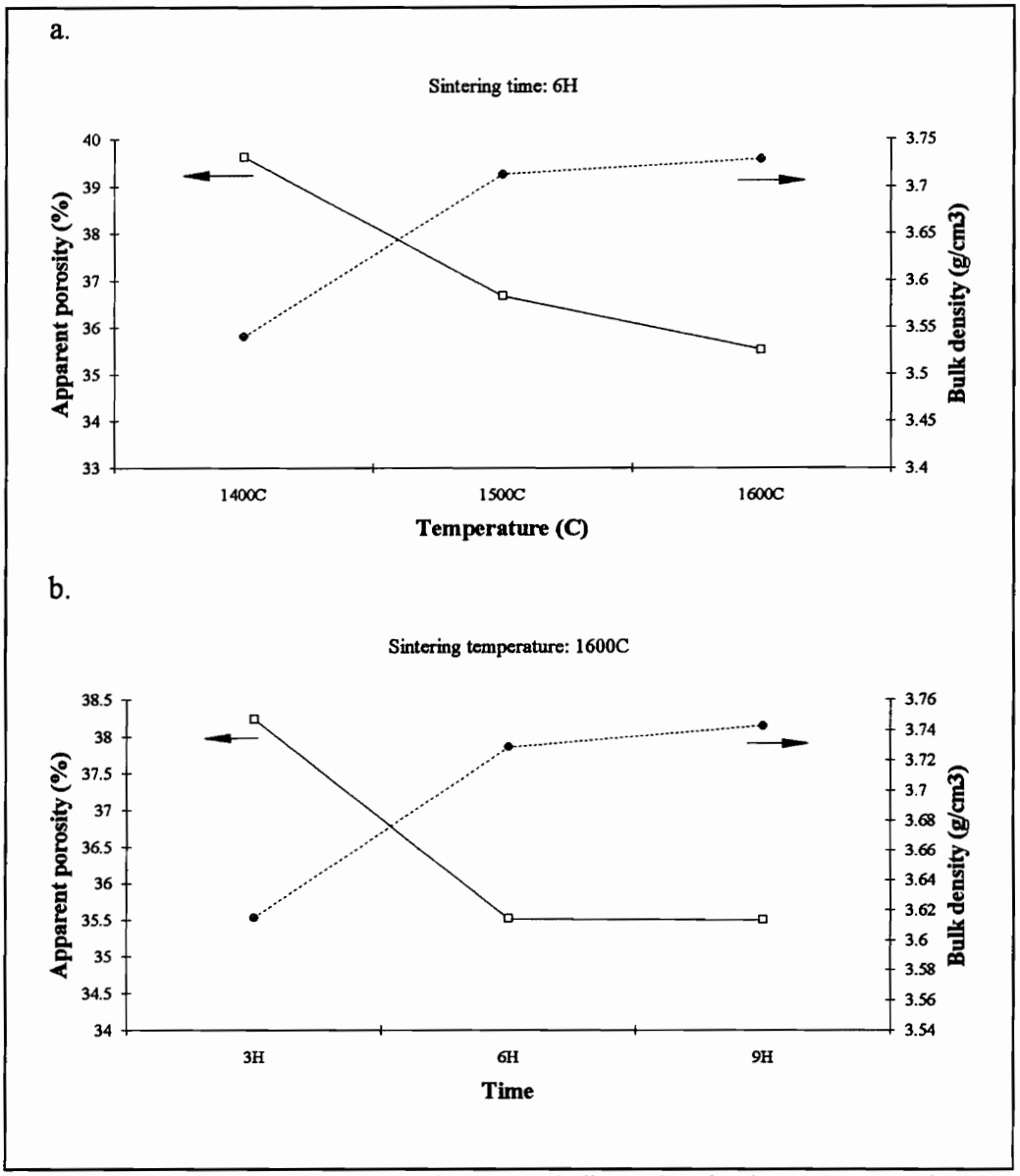

Figure 3.6: Variation of the apparent porosity and the bulk density of YSZ samples as a function of a) the temperature of sintering, and b) the time of sintering

3.2.3. DENSITY AND POROSITY MEASUREMENT.

The bulk density of the samples were determined using the water displacement method, ASTM C2087. Relative density was then calculated by taking the ratio of the bulk density to the theoretical density (8.9 g/cm^3 for Bi_2O_3 and 5.7 g/cm^3 for YSZ).

The bulk density of the Bi_2O_3 samples was estimated to 7.7±0.2 g/cm^3 and led to a relative density of 86±2 %.

The determination of the bulk density of the YSZ samples gave a value 3.75±0.3 g/cm^3 corresponding to a relative density of 66±5 %.

The water displacement method also permits apparent porosity calculations. These calculations suggest approximately 18% of apparent porosity in the Bi_2O_3 samples and 35.5% in the YSZ samples.

3.2.4. MICROSTRUCTURE CHARACTERIZATION.

An International Scientific Instruments ISI-SX-40 scanning electron microscope (SEM) was used to study the microstructures of the samples. The sintered cylinders were intentionally fractured and the fracture surfaces were polished and etched with hydrofluoric acid for 10 seconds to make the grain boundaries discernible. The surfaces were then observed and an example of a micrograph of both types of samples is illustrated in Figs. 3.7 and 3.8.

The grain sizes of the samples were measured from these micrographs by the planimetric (or Jeffries') procedure in the ASTM E112-88. Bismuth oxide samples exhibited equiaxed grains of 9 μm, and the yttria-stabilized samples were characterized by a grain size of 27 μm.

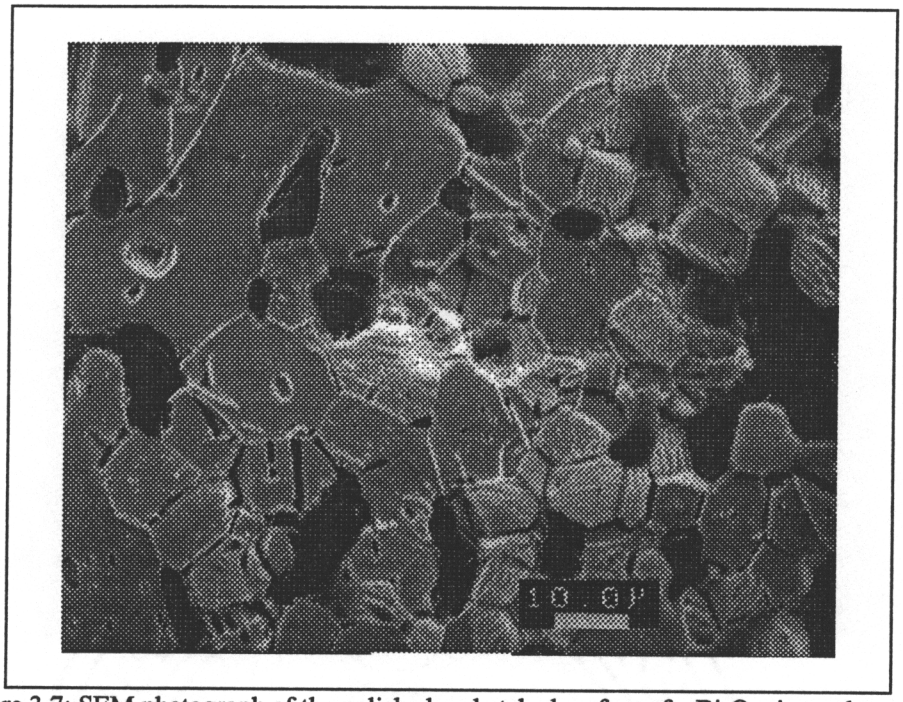

Figure 3.7: SEM photograph of the polished and etched surface of a Bi_2O_3 sintered sample.

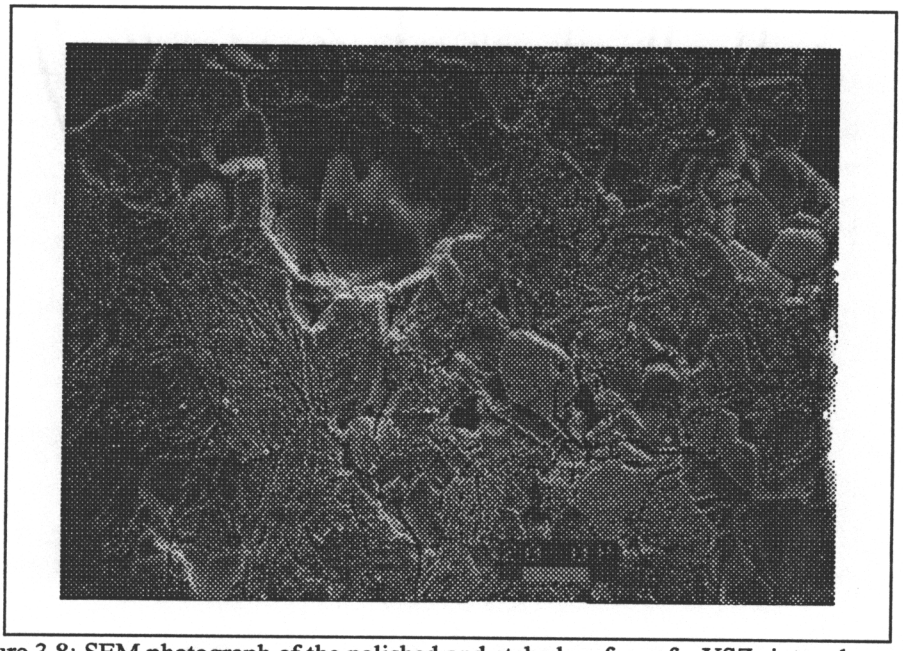

Figure 3.8: SEM photograph of the polished and etched surface of a YSZ sintered sample.

4. CHARACTERIZATION OF SUPERPLASTIC BEHAVIOR

In the previous literature, structural superplastic behavior has been put to fore mostly through investigations utilizing compression or tensile tests [13,14,18-20,22-30]. In this study, compression testing was the prefered method of characterization because of limitations in sample processing. The most important one of these was due to the length-diameter ratio limitation of the cold pressing process. As a result, tensile test specimens from ceramic-based materials would be extremely difficult to prepare, whereas the compression test sample shape was more easily achievable.

4.1. METHODOLOGY OF THE COMPRESSION TESTS

Superplasticity was previously defined as large deformation accompanied by a high strain rate sensitivity and characterized by the following equation:

$$\sigma = B\dot{\varepsilon}^m, \tag{2.1}$$

which can also be written as

$$\log(\sigma) = m \log(\dot{\varepsilon}) + \log(B). \tag{4.1}$$

As a consequence, for a material with a constant microstructure, i.e. a constant B, the flow stress (σ) can be obtained by constant strain-rate tests. These tests are highly appropriate to characterize superplastic behavior and consist of measuring the steady-state load for a range of strain rates, $\dot{\varepsilon}$, plotting $\log(\sigma)$ as a function of $\log(\dot{\varepsilon})$, and finally calculating m from the slope of the curve obtained. Due to the difficulty in obtaining low strain rates, constant strain-rate tests can be substituted by constant load or constant-stress

creep tests in which the steady strain rate is measured as a function of the applied load [2]. Due in part to the availability of necessary equipment, most superplastic data available in the literature have been obtained using the constant crosshead speed approach.

4.1.1. CONSTANT CROSSHEAD SPEED TEST

In this study, compression tests with constant crosshead speed were carried out on an Applied Test System (ATS) machine (Fig. 4.1) to determine the superplastic behavior of the bismuth oxide and stabilized zirconia samples.

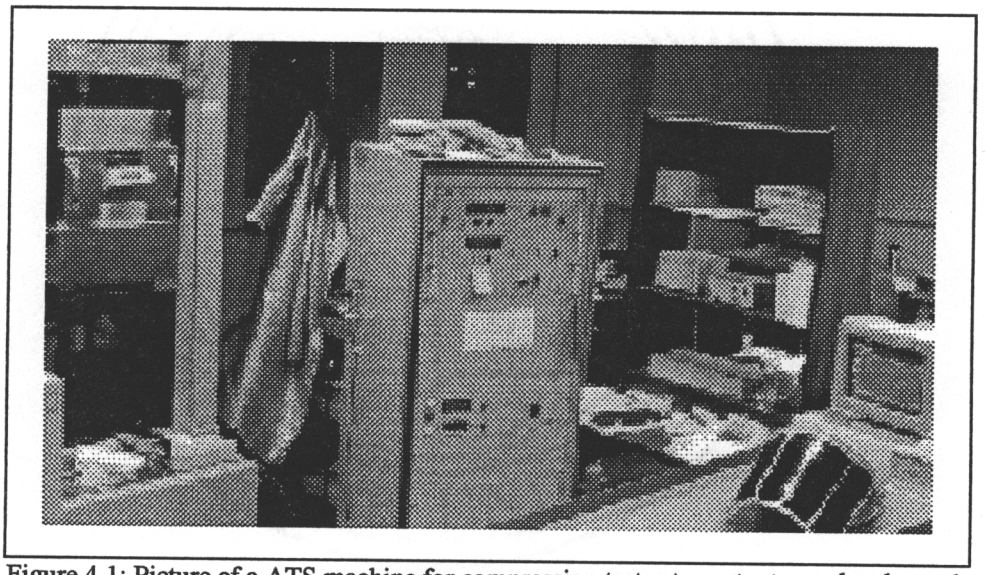

Figure 4.1: Picture of a ATS machine for compression tests at constant crosshead speed.

The output data given by this equipment during test performance were the instantaneous displacement, $\Delta L(t)$, and the corresponding applied load, $P(t)$. The displacement is converted to the true strain, ε, by the following relations:

$$\varepsilon = \ln\left(\frac{L(t)}{L_0}\right) \tag{4.2}$$

where L_0 is the initial length of the sample,

and $L(t)$ is the instantaneous length of the sample, i.e., $L(t) = L_0 - \Delta L(t)$.

Hence,

$$\varepsilon = \ln\left(1 - \frac{\Delta L(t)}{L_0}\right). \tag{4.3}$$

Similarly, the load is converted to the true stress, $\sigma(t)$:

$$\sigma(t) = \frac{P(t)}{A(t)} \tag{4.4}$$

where $A(t)$ is the instantaneous cross-sectional area of the sample.

If we consider the deformations as fully plastic, we can assume that the volume of the sample remains constant, i.e., affine deformations, and, thus,

$$A(t)\cdot L(t) = A_0 \cdot L_0 \tag{4.5}$$

where A_0 is the initial cross sectional area.

So,
$$\sigma(t) = \frac{P(t)\cdot L(t)}{A_0 \cdot L_0}, \tag{4.6}$$

and finally

$$\sigma(t) = \frac{P(t)}{A_0}\left(1 - \frac{\Delta L(t)}{L_0}\right). \tag{4.7}$$

The strain rate, $\dot{\varepsilon}$, is derived from equation (4.2):

$$\dot{\varepsilon} = \frac{\delta\varepsilon}{\delta t} = \frac{\dot{L}}{L(t)} \tag{4.8}$$

and can also be referred to the displacement:

$$\dot{\varepsilon} = \frac{\cdot\, \dot{L}}{L_0 - \Delta L(t)} \tag{4.9}$$

where $\dot{L}$ is the crosshead velocity.

In order to characterize the superplasticity of our samples, compression tests were performed for different crosshead speeds at different temperatures. Since enhanced deformations have been observed in superplastic materials for strain rates in the order of magnitude of 10^{-4} s^{-1} [2,13,14,18-20], the crosshead speeds were determined according to the capacity of the equipment and the length of our samples, so that the initial strain rate, $\dot{\varepsilon}_0$, was as close to this value as possible.

From equation (4.9), we have $$\dot{\varepsilon}_0 = \frac{\dot{L}}{L_0} \tag{4.10}$$

with $\dot{L}$ from 0.005 to 0.3 in/min or 0.002 to 0.127 mm/s,
and L_0 from 15 mm (at room temperature) to 20 mm (at higher temperature with the thermal expansion).

As a result, $\dot{\varepsilon}_0$ varied from 1.06×10^{-4} to 8.47×10^{-3} s^{-1}.

For each choice of temperature and crosshead velocity, the true stress was plotted as a function of the true strain. When superplastic behavior was observed, i.e., a deformation of 50% or more, the approximately constant flow stress and the corresponding mean strain rate were recorded. Then, for each temperature, the variation of the flow stress with the strain rate was reported on a graph with logarithmic scale. According to equation (4.1),

the slope of the traced curve gives the value of the strain rate sensitivity, m. Finally, the activation energy for superplastic flow, Q_c, can be evaluated by two distinct ways assuming that m remains constant over the temperature range employed: Q_c can be derived either from the slope ($-Q_c/R$) of the strain rates versus the inverse temperature curves at constant stress, or from the slope (mQ_c/R) of the flow stress versus the inverse temperature curves for constant strain-rate, according to the equation:

$$\dot{\varepsilon} = AD_0 \exp(-\frac{Q_c}{RT})(\frac{1}{d})^p \sigma^n. \qquad (2.2)$$

4.1.2. VELOCITY JUMP TEST

Whereas most of the data on superplasticity available in the literature comes from constant crosshead speed tests, they cannot be considered as truly representative of the steady-state [2]. Furthermore, the strain rate is not a constant. As the length of the sample decreases, the rate increases following equation (4.8). Similarly, the value of the flow stress is raised following equation (2.1). In addition, the microstructure of the samples is often unstable at temperatures where the tests are performed ($T > 0.5\ T_{MP}$). For example, grain growth may occur leading to an increase in the flow stress. In an effort to avoid this dilemma, a variation of the compression test configuration, the velocity jump test, was adopted. This type of test, first developed by Backofen et al. [12], is based on the same method used for constant crosshead speed tests. The compression testing is performed at a fixed temperature and at a constant speed until a steady state deformation is obtained. The characteristic of the jump tests is the fact that when this point is attained, the velocity of the crosshead is raised or lowered and maintained at its new value to allow

the load to stabilize in a new steady state. This operation is then repeated as long as a constant flow stress is achievable.

When enhanced deformations were observed with constant crosshead speed tests, several velocity jump tests were performed at different temperatures to evaluate the characteristics of the superplasticity of the materials, i.e., the strain rate sensitivity m and the activation energy Q_c. Then, the displacement and the load are converted respectively to the true strain and the true stress using the same equations ((4.3) and (4.7)) as for the constant crosshead speed tests. Finally, the flow stress was reported as a function of the mean strain rate and the data were analyzed according to the procedure desribed previously.

4.2. RESULTS FOR THE BISMUTH OXIDE SAMPLES

4.2.1. TESTS AT ROOM TEMPERATURE

In order to analyze the high temperature behavior of our Bi_2O_3 samples, compression tests were first performed at room temperature. The slowest crosshead speed, i.e., 0.005 in/min or 0.002 mm/s, corresponding to an initial strain rate of 1.41×10^{-4} s^{-1}, was selected and five samples were tested. A catastrophic fracture of each of the samples occurred after a small amount of deformation. The resulting true stress versus true strain curve is plotted in Fig. 4.2.

Several conclusions can been drawn from this curve. First, it is characteristic of a brittle material since essentially no plasticity was observed. Secondly, two regions with differening slopes can be distinguished on the plot. The presence of the initial slope can be explained by some inevitable misalignment of the sample and testing fixtures as the test

started. Finally, several mechanical properties can be deduced like the Young modulus and the compression strength. The fracture strength is the maximum stress reached , i.e., 23.5 MPa, and the Young modulus, E, calculated from the slope of the curve, is 1175 MPa.

The fracture surface of the tested samples has been also observed with a scanning electron microscope (SEM) and is illustrated in Fig. 4.3. In this micrograph, few grains are visible and most of the grain boundaries are not discernible. As a consequence, the surface was polished, etched with hydrofluoric acid for 10 seconds and observed again. This procedure rendered the grain boundaries visible and the hexagonal shape of the grains was put to the fore, Fig. 4.4.

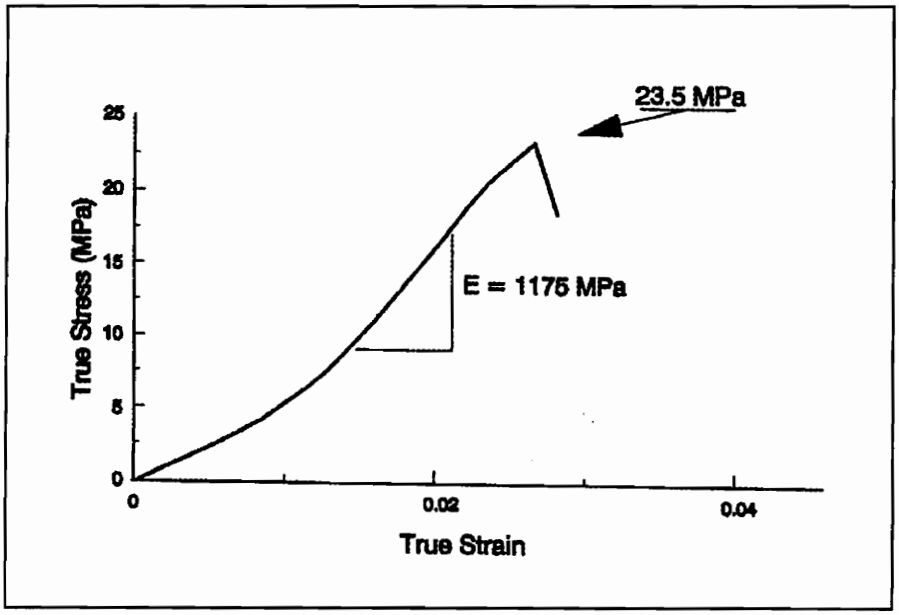

Figure 4.2: True stress-true strain curve of the compression test of a Bi_2O_3 sample at room temperature with an initial strain-rate of $1.41 \times 10^{-4}\ s^{-1}$.

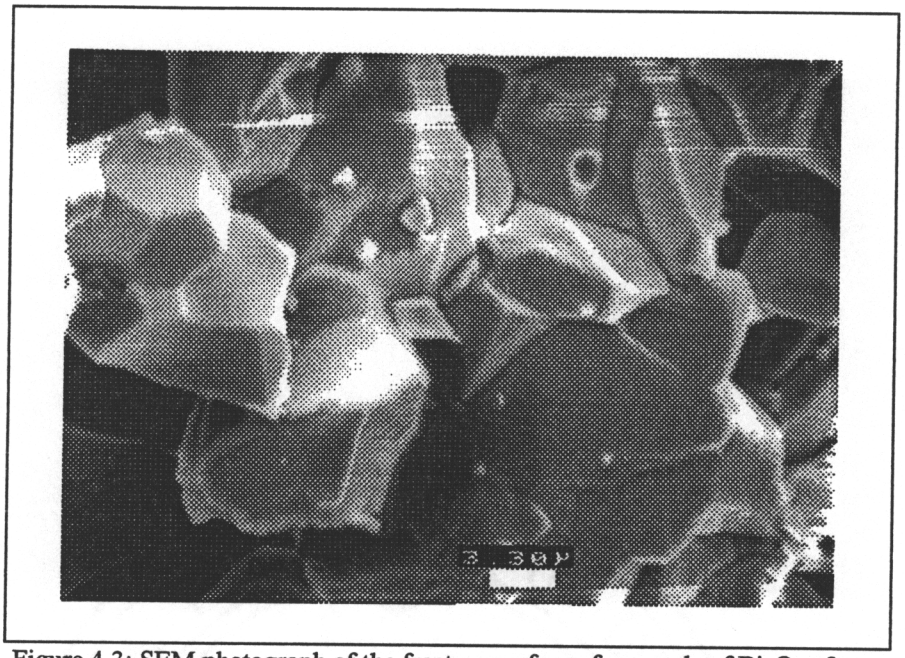

Figure 4.3: SEM photograph of the fracture surface of a sample of Bi_2O_3 after a compression test at room temperature.

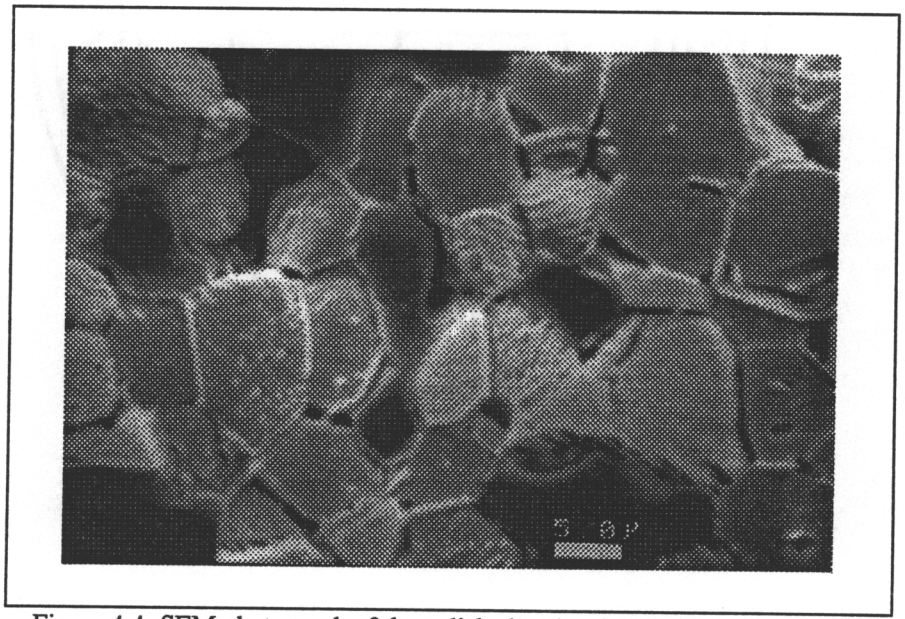

Figure 4.4: SEM photograph of the polished and etched fracture surface of a sample of Bi_2O_3 after a compression test at room temperature.

4.2.2. TESTS AT HIGH TEMPERATURE ($T > 0.5T_{MP}$).

Bismuth oxide, known for its transformational superplasticity associated with the transition from its monoclinic to its cubic phase [7], has never been documented as exhibiting structural superplasticity in either of these two phases. Nevertheless, if an analogy is made with pure zirconia, for which transformational superplasticity was first discovered through the monoclinic to tetragonal phase transition in 1967 [21], and later, structural superplasticity in its tetragonal phase [13,14,18-20,23-30], structural superplasticity is likely to be observed in δ-Bi_2O_3. Several initial tests were performed to determine if the bismuth oxide cubic phase was superplastic.

First, compression tests were performed at 700°C, a temperature for which Bi_2O_3 is still in its monoclinic phase, utilizing the same crosshead speed used in the room temperature tests. The failure of the slightly deformed samples occured in a brittle manner with the formation of multiple cracks. The results of these tests are represented Fig. 4.5.

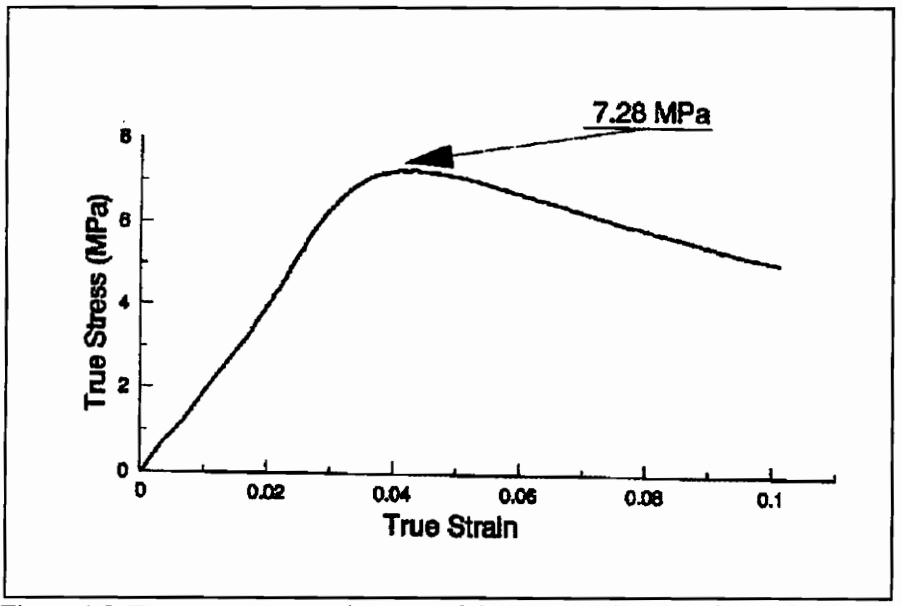

Figure 4.5: True stress-true strain curve of the compression test of a Bi_2O_3 sample at 700°C with an initial strain-rate of $1.18 \times 10^{-4}\ s^{-1}$.

The shape of the curve shown in Fig. 4.5 is comparable to the one obtained at room temperature, i.e., no plasticity is observed. The true strain before fracture is raised to almost 0.04 but the compression strength dropped to 7.3 MPa (from 23.5 MPa at room temperature) and the Young modulus to 182 MPa (from 1175 MPa). According to these data, the α-Bi_2O_3 did not exhibit any superplastic behavior.

Secondly, the same tests were performed at 750°C, above the transition temperature (730°C), in the cubic phase. Even though the porosity of the samples was high, deformations of more than 85% (engineering strain) were observed without rupture. The specimen, initially ∅10x15 mm cylinders, became pellets of approximately ∅20x3 mm, as illustrated in Fig.4.6. The magnitude of the deformation obtained at constant temperature, i.e., with no cycling through the monoclinic to cubic phase transition, strongly suggests the presence of structural superplasticity.

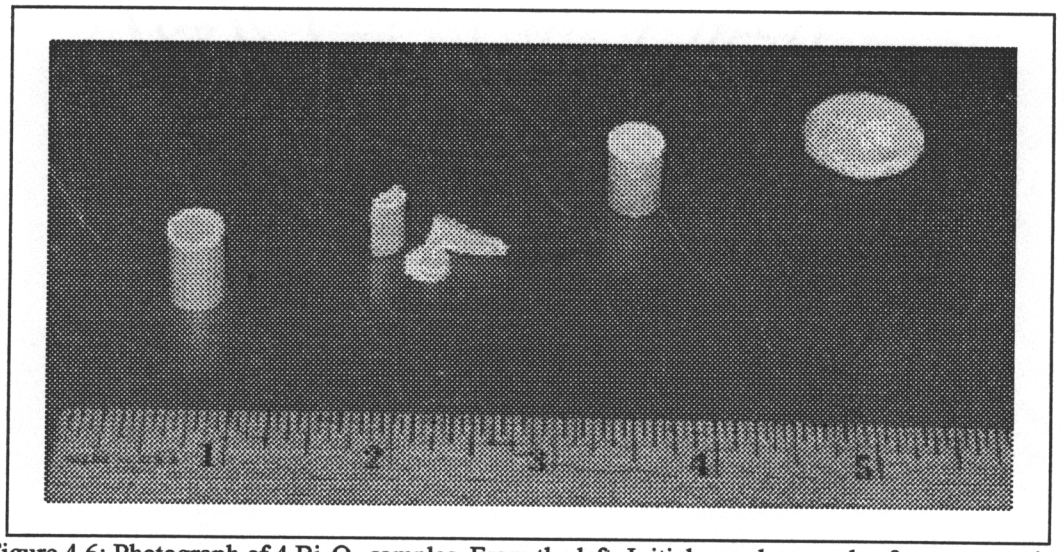

Figure 4.6: Photograph of 4 Bi_2O_3 samples. From the left: Initial sample, sample after compression test at room temperature, sample after compression test at 700°C and sample after compression test at 750°C.

The shape of the true stress versus the true strain obtained for the superplastic material is illustrated by Fig. 4.7. The steady-state flow stress of 0.95 MPa (almost eight times lower than the compression strength measured at 700°C) was achieved at approximately 0.1 of true strain.

Additional tests were conducted at 775°C and 800°C to verify the structural superplasticity observed at 750°C . In each of these instances, steady state flow stress was attained at strains less than 0.1, with decreases in the magnitude of the flow stress with increasing temperatures. Increasing the strain-rate from 1.06×10^{-4} s^{-1} to 3.18×10^{-4} s^{-1} at 775°C led to similar behavior. These results are illustrated in Fig. 4.8 and can be summurized by noting that the flow stress is lowered by either an increase in the temperature and/or by a decrease in the strain-rate.

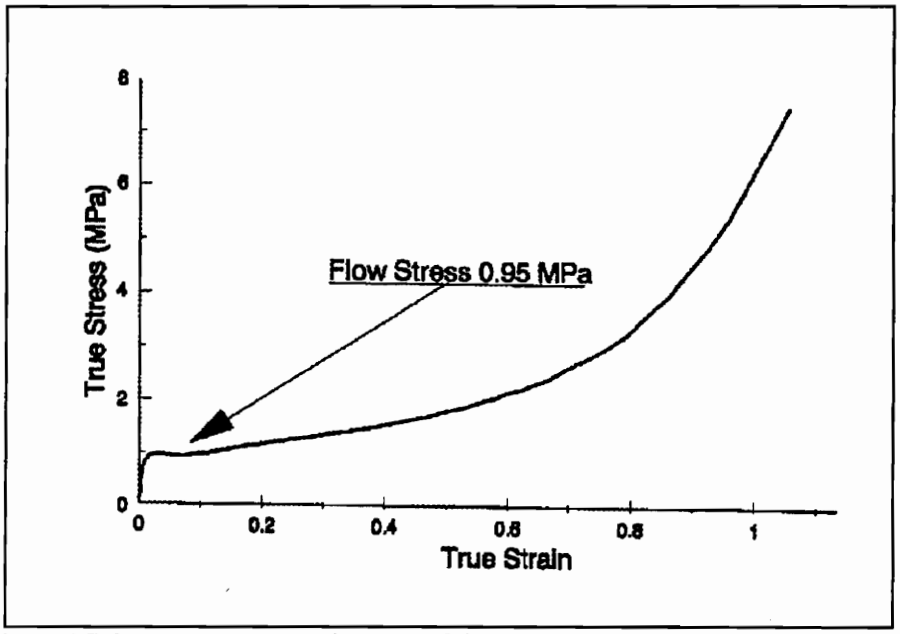

Figure 4.7: True stress-true strain curve of the compression test of a Bi_2O_3 sample at 750°C with an initial strain-rate of 1.06×10^{-4} s^{-1}.

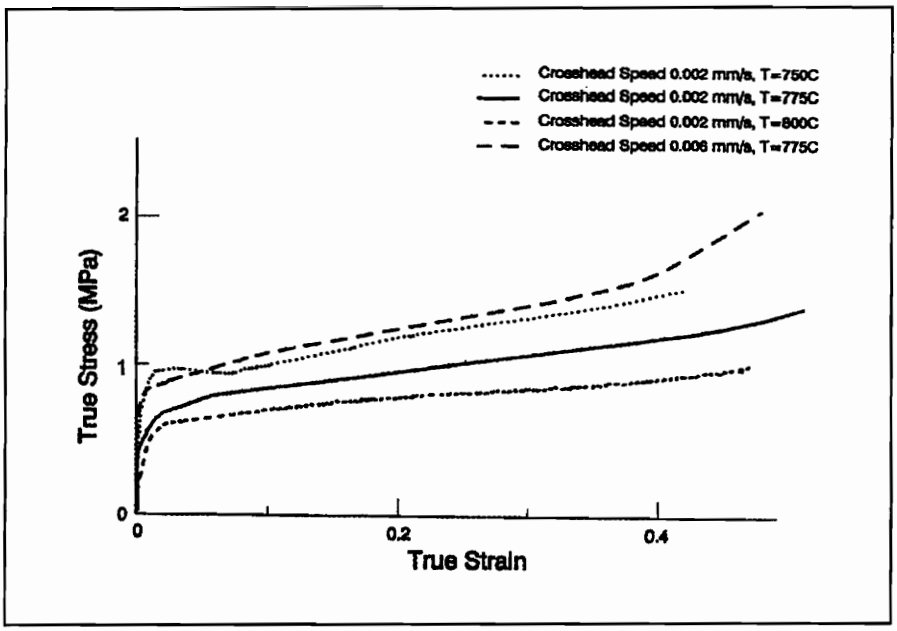

Figure 4.8: Effect of the temperature and the crosshead speed on the true stress-true strain curve of the compression test of a Bi_2O_3 sample.

After each test, the deformed samples were purposely fractured and the interior surfaces were observed using SEM. The microstructures of the samples at these temperatures were significantly different from that obtained at room temperature, as shown in Fig. 4.9. The first difference was that the grain boundaries are clearly visible and neither polishing nor etching is necessary. The second difference was in the shape of the grains. Whereas grain shape remained constant during room temperature tests, two distinctive regions were apparent for the superplastic samples. In one instance, Fig. 4.9a, the grains retained their original shape and size. Conversely, regions were also present which exhibited highly elongated grains.

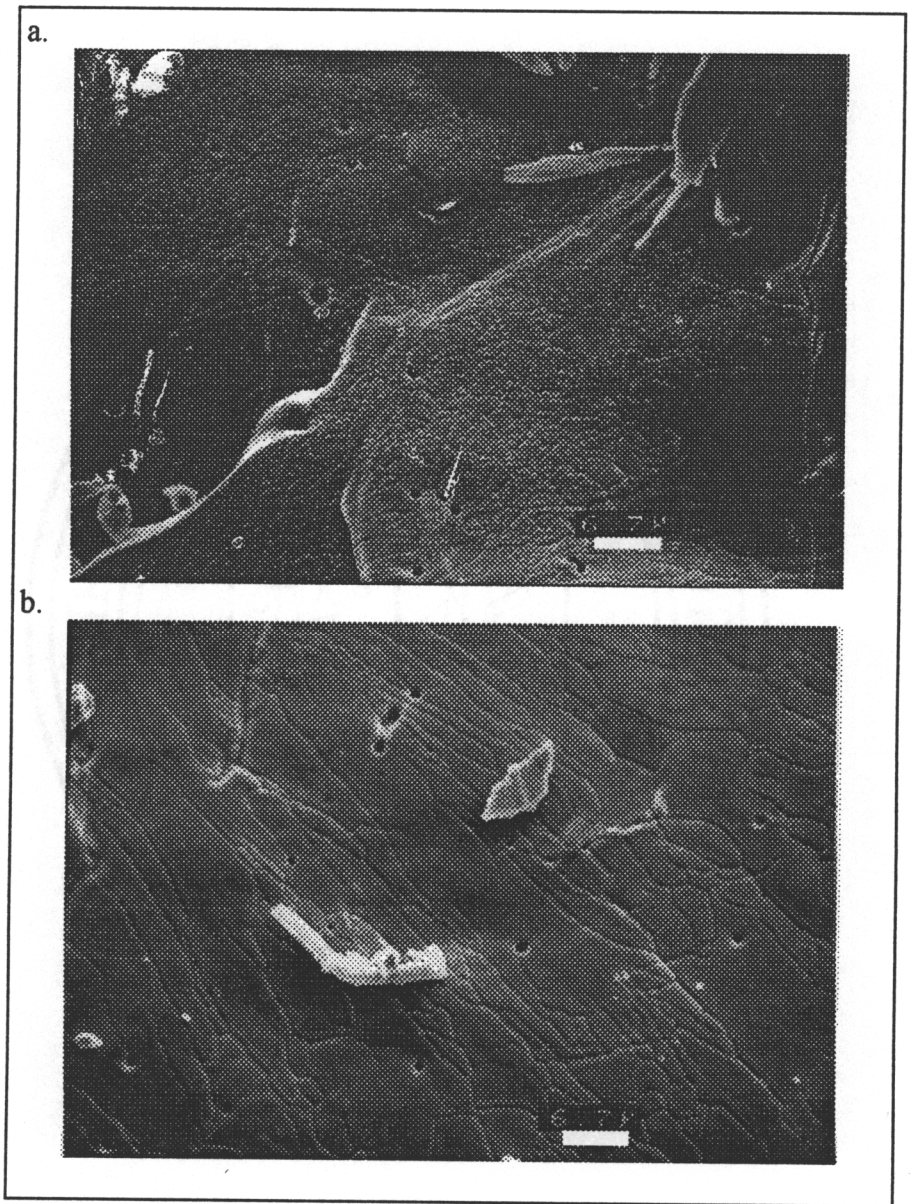

Figure 4.9: SEM photograph of the fracture surface of a Bi_2O_3 sample deformed superplastically: a) undeformed grains, b) elongated grains.

Whereas the proof of the structural superplasticity of bismuth oxide was easily made by constant crosshead speed tests, the strain rate sensitivity and the activation energy were calculated from the results of velocity jump tests at different temperatures.

The magnitudes of the strain-rate changes (jumps) were determined so that the response of the flow stress to strain-rate changes could be easily discerned. As a result, the following crosshead speeds were chosen:

0.005 - 0.01 - 0.015 - 0.03 - 0.06 - 0.12 in/min

or 0.002 - 0.004 - 0.006 - 0.013 - 0.025 - 0.051 mm/s.

We should note that a steady-state was not always achieved for the highest speed. When this occurred, the last velocity jump was ignored, i.e., only steady state flow stresses were used in the calculations.

Jump tests were performed on four samples at three distinct temperatures, i.e., 750°C, 775°C, and 800°C. The deformations and the changes in the microstructure generated through these tests were comparable to those observed with the previous constant crosshead velocity tests. An example of the derived true stress-true strain curves is illustrated for each of the temperatures examined and are shown in Figs. 4.10, 4.11, and 4.12.

The flow stresses obtained through these tests were compared to those obtained for the corresponding constant crosshead speed test. To illustrate this comparison, Fig. 4.13 represents two tests run at 775°C. The first one is a constant crosshead speed test with an initial strain-rate of 3.18×10^{-4} s^{-1}, i.e., a crosshead velocity of 0.015 in/min, and the second one a jump test. The jump test gives a flow stress of 1.32 MPa when the crosshead speed is 0.015 in/min while the flow stress obtained through the other test is 1.11 MPa. The two values are relatively close and can lead to the conclusion that the flow stress is only slightly dependent on the strain.

From the different true stress-true strain curves, the flow stresses and their corresponding strain rate were noted each time a steady state stress was attained. The acquired data were then plotted on a logarithmic scale. The shape of the resulting flow stress-strain rate curves were linear as predicted by expression (4.1). A linear regression was effected on each plot and the determination of their slope gave the value of the strain-rate sensitivity, m, which varied from 0.27 to 0.35. For each temperature, the data from the four performed tests were grouped and the average value of m was obtained. As an illustration, Figs. 4.14, 4.15, and 4.16 represent the flow stress-flow strain curves, respectively at 750°C, 775°C, and 800°C, on which the linear regression and its 95% confidence interval have been plotted.

The average flow stress calculated from the mean values of the determined power law constants as a function of strain-rate for all three tests temperatures is shown in Fig.4.17. This plot exhibits a slight dependence of the strain-rate sensitivity with the temperature and the slope of the 775°C data seems to be larger than the two other ones. This tendancy is further illustrated by Fig. 4.18. The mean value of m was found to be 0.29 at 750°C, 0.33 at 775°C, and 0.32 at 800°C.

Calculation of activation energy for thermally-activated deformation processes necessitates a constant value of m over the temperature range of interest. While this is not strictly obeyed in the present data (Fig. 4.18), the experimental values of m are sufficently similar in magnitude such that an estimate of the activation energy can be calculated and a mean value was evaluated at 0.3133 from the complete data acquired during the different tests performed as shown in Fig. 4.19.

Figs. 4.20 and 4.21 represent two approaches for calculating Q. In Fig. 4.20, strain-rate has been illustrated as a function of inverse temperature; the activation energy is obtained from the slope from equation (2.2) according to

$$\left.\frac{\delta \ln \dot{\varepsilon}}{\delta(1/T)}\right|_{d,\sigma,m} = -\frac{Q}{R}. \qquad (4.11)$$

Similarly, activation energy can also be calculated by differentiating equation (2.2) according to

$$\left.\frac{\delta \ln \sigma}{\delta(1/T)}\right|_{d,\dot{\varepsilon},m} = m\frac{Q}{R}. \qquad (4.12)$$

Average activation energy is calculated to be approximately 157,000±36,000 J/mol (1.6 ±0.4 eV) as per equation (4.11) and approximately 145,000±24,000 J/mol (1.5±0.2 eV) by the latter method.

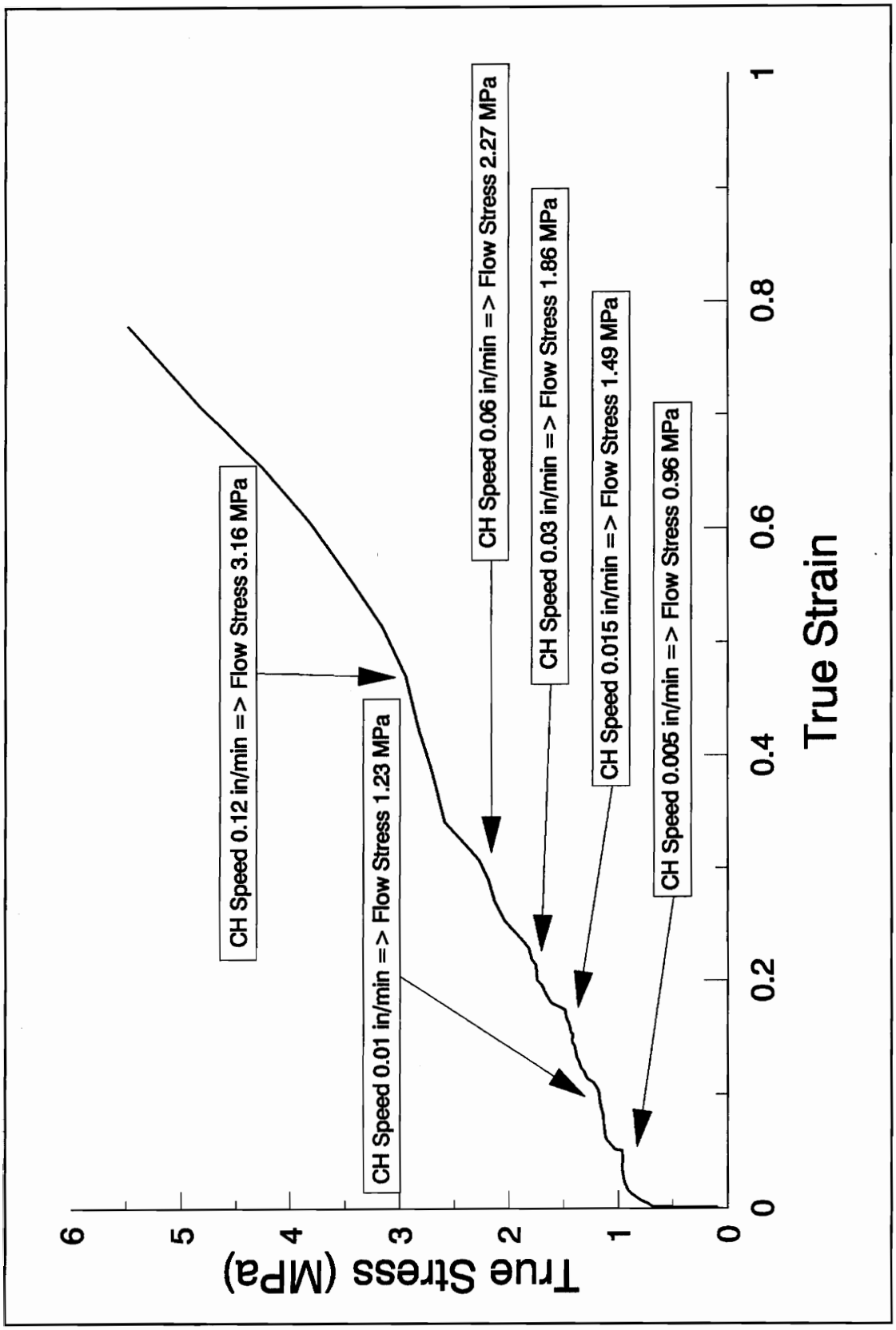

Figure 4.10: True stress - true strain curve from the compression jump test of a Bi_2O_3 sample at 750°C.

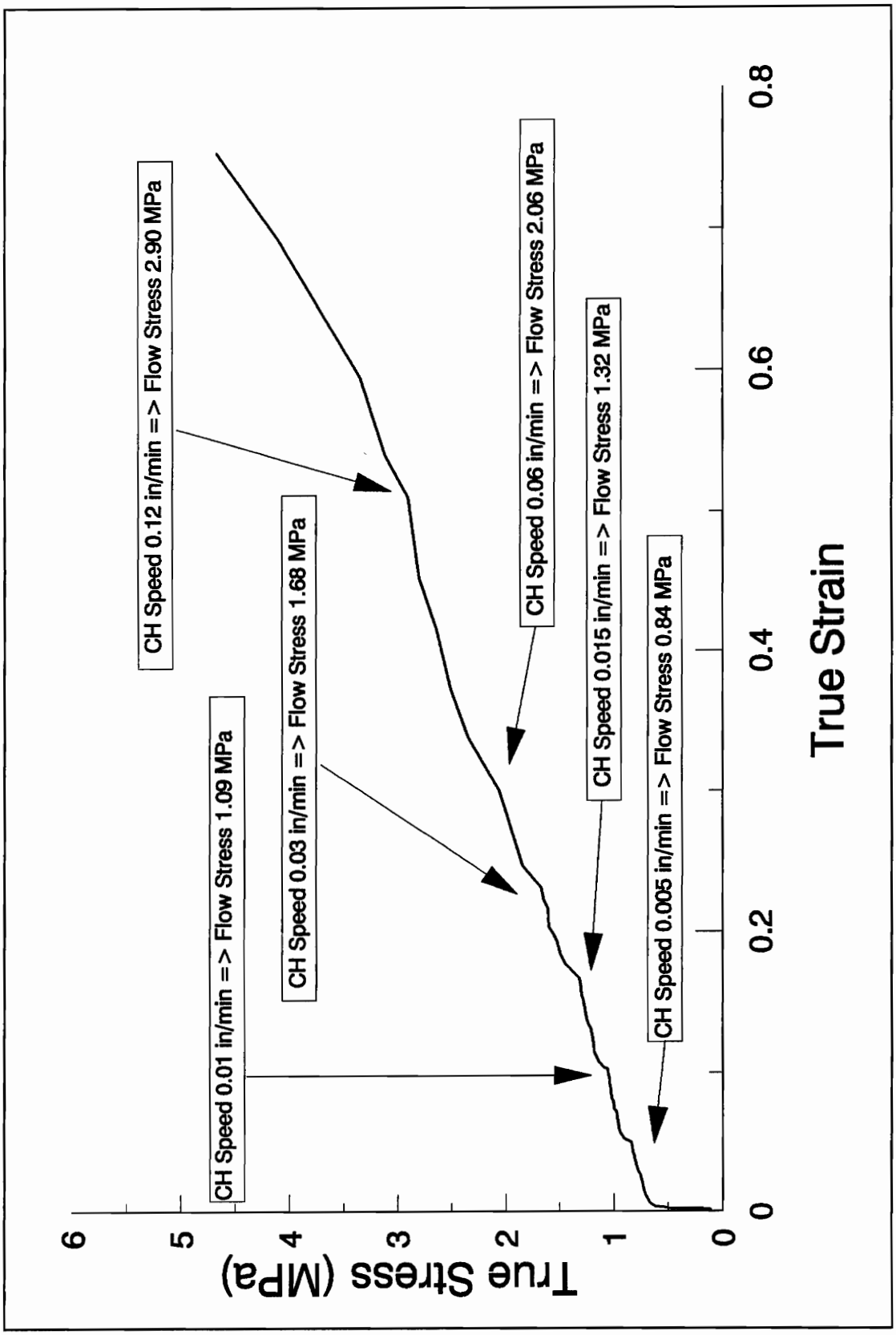

Figure 4.11: True stress - true strain curve from the compression jump test of a Bi_2O_3 sample at 775°C.

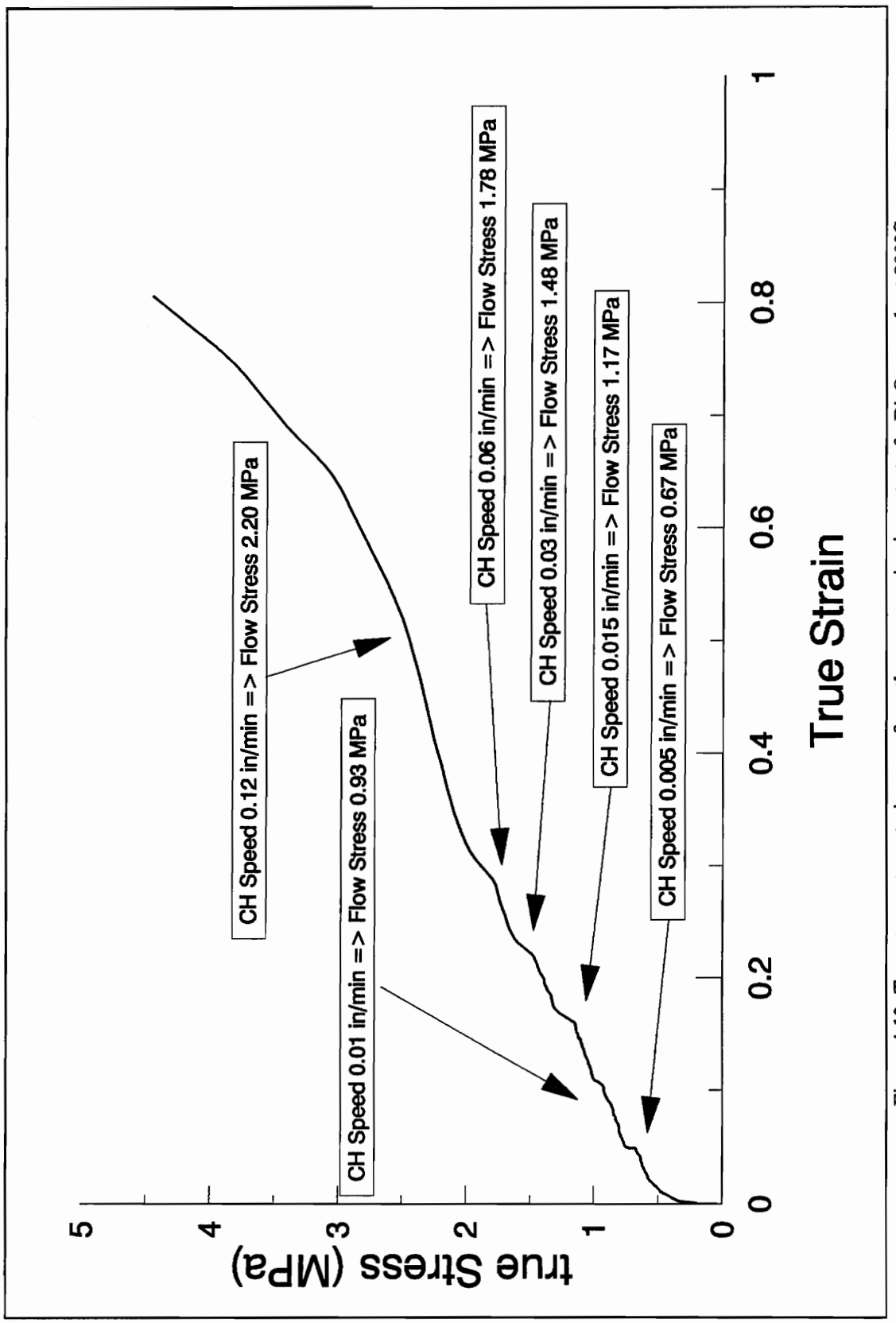

Figure 4.12: True stress - true strain curve from the compression jump test of a Bi_2O_3 sample at 800°C.

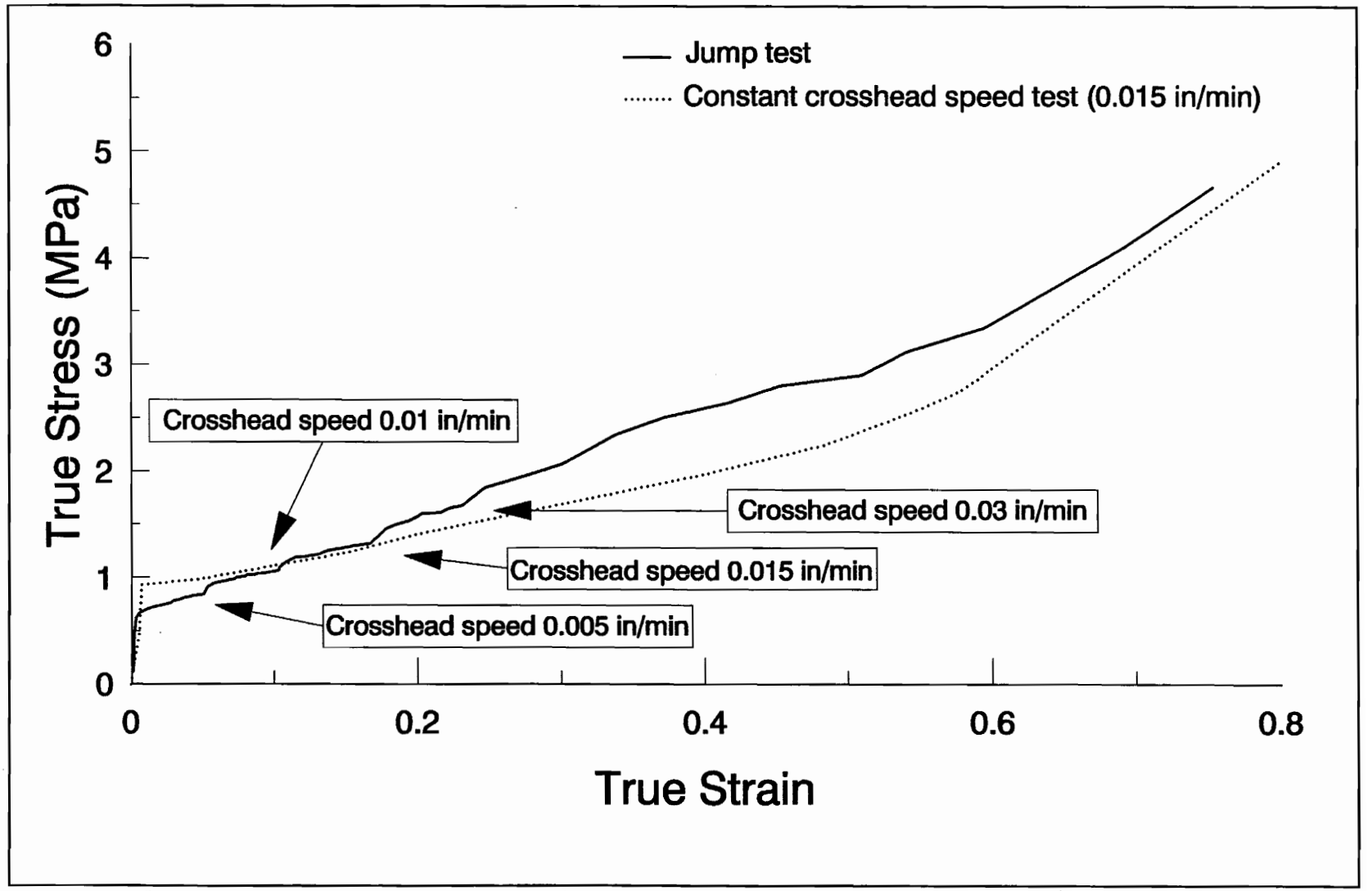

Figure 4.13: Comparison between a constant crosshead speed compression test, with an initial strain-rate of 3.18×10^{-4} s^{-1}, and a compression jump test of a Bi_2O_3 sample at 775°C.

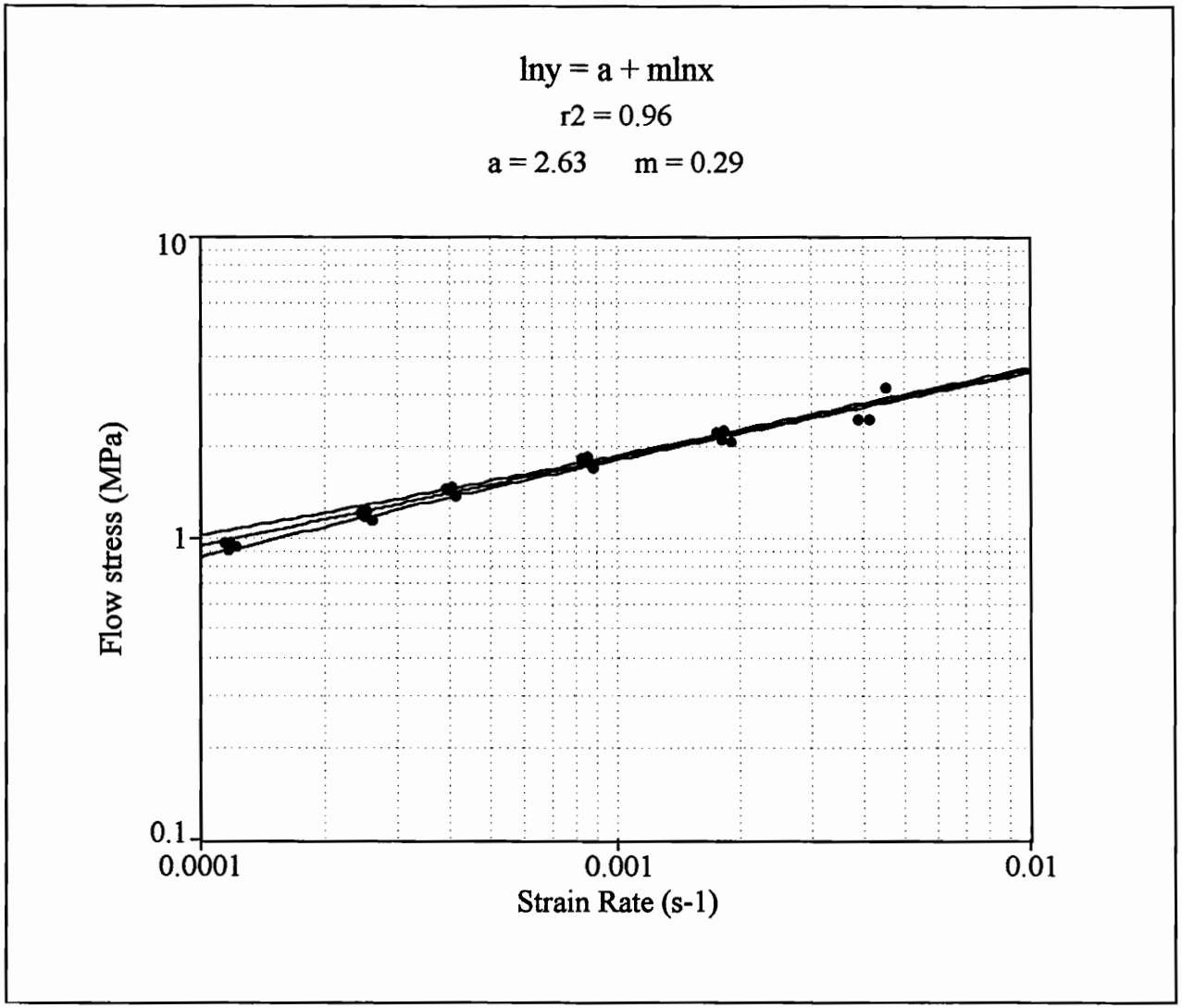

Figure 4.14: Flow stress - strain-rate curve from the compression jump test of a Bi_2O_3 sample at 750°C. Shown are the lines corresponding to regression analysis (interior line) and the 95% confidence limits (bounding lines).

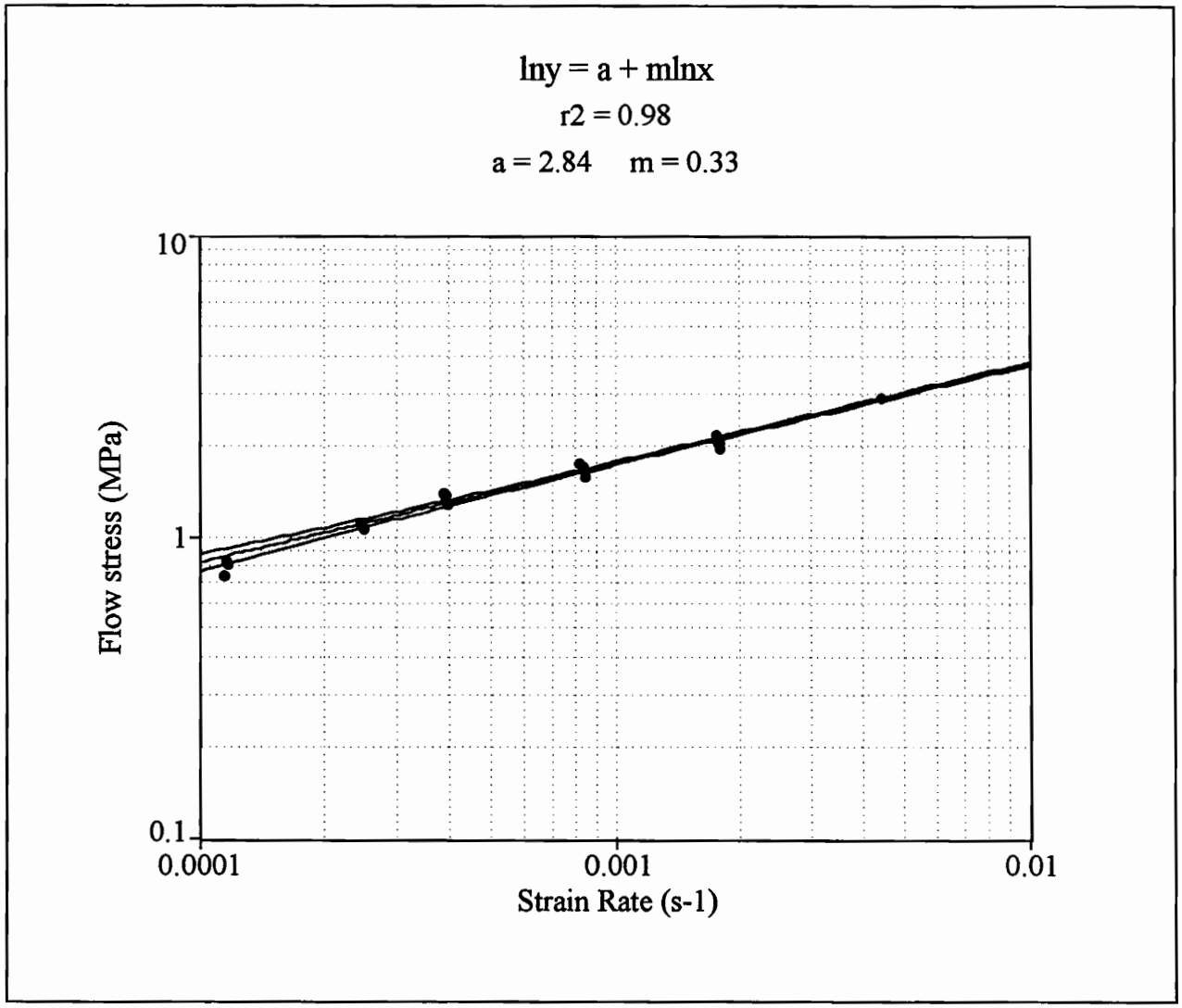

Figure 4.15: Flow stress - strain-rate curve from the compression jump test of a Bi_2O_3 sample at 775°C.
Shown are the lines corresponding to regression analysis (interior line) and the 95% confidence limits (bounding lines).

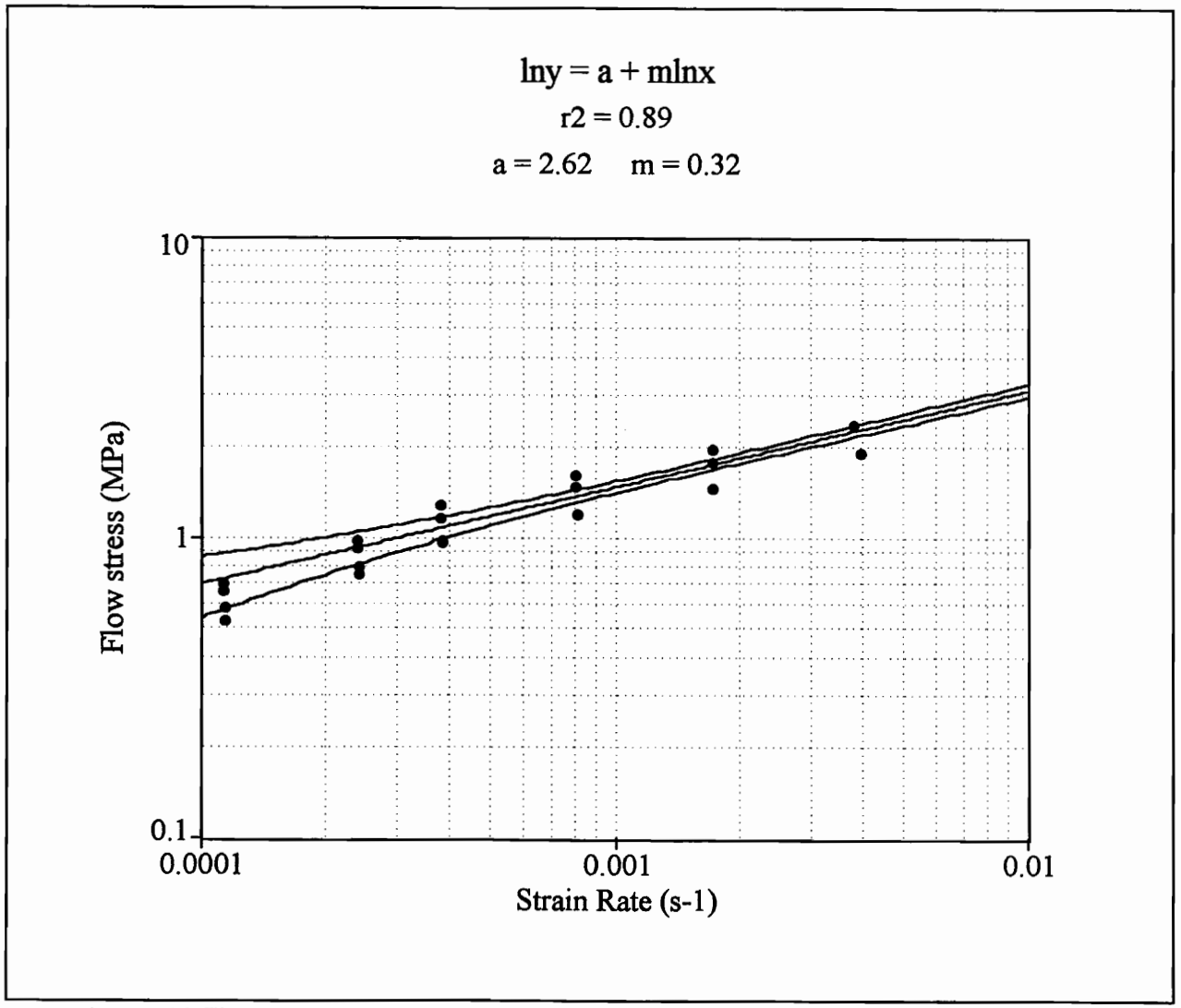

Figure 4.16: Flow stress - strain-rate curve from the compression jump test of a Bi_2O_3 sample at 800°C. Shown are the lines corresponding to regression analysis (interior line) and the 95% confidence limits (bounding lines).

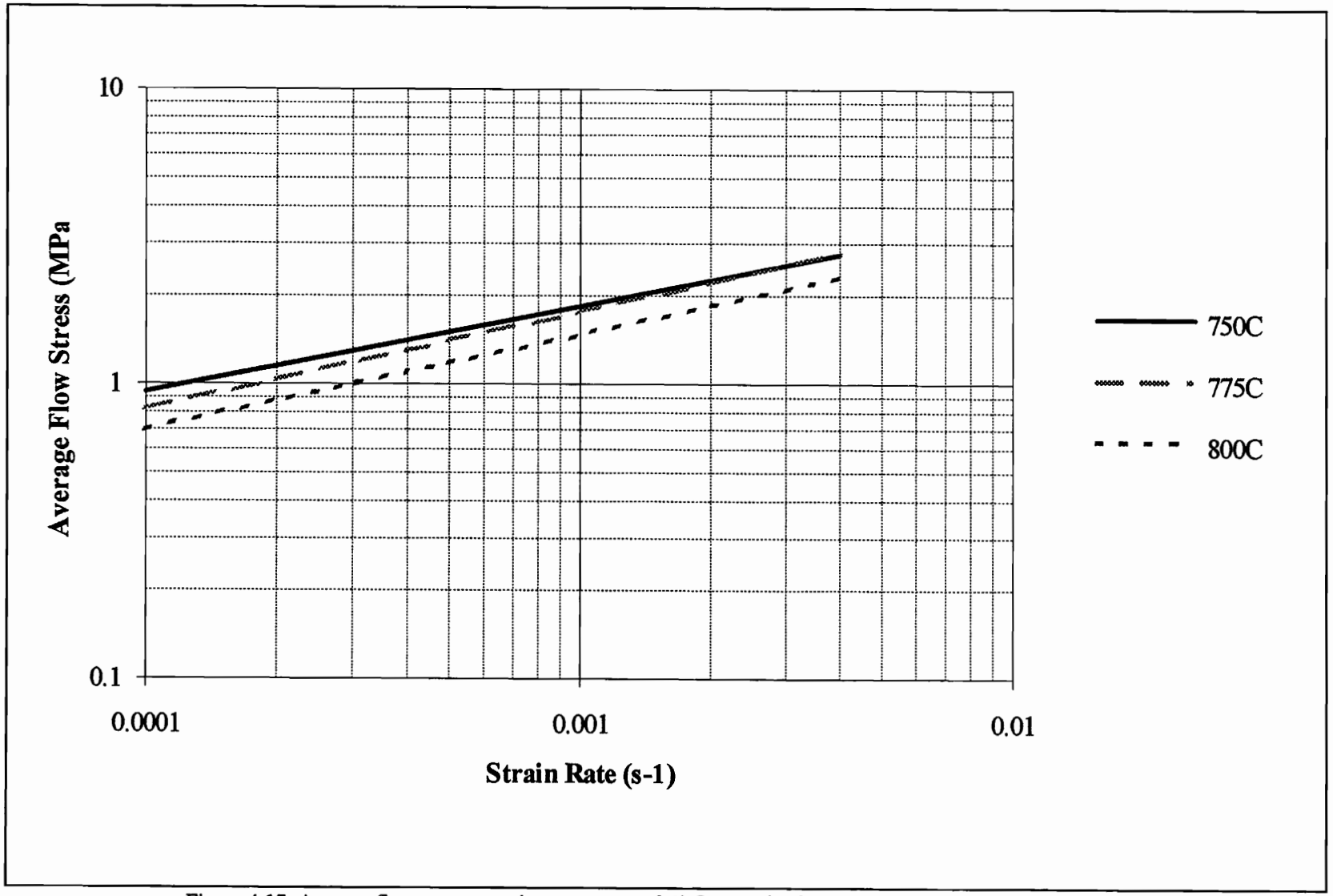

Figure 4.17: Average flow stress - strain-rate curves of Bi_2O_3 samples for temperatures of 750, 775, and 800°C.

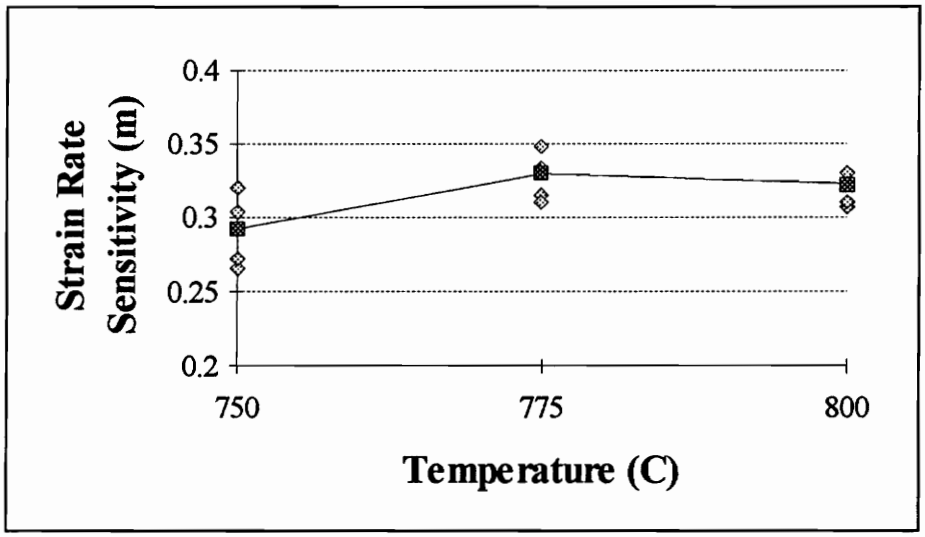

Figure 4.18: Strain-rate sensitvity of Bi_2O_3 samples as a function of temperature.

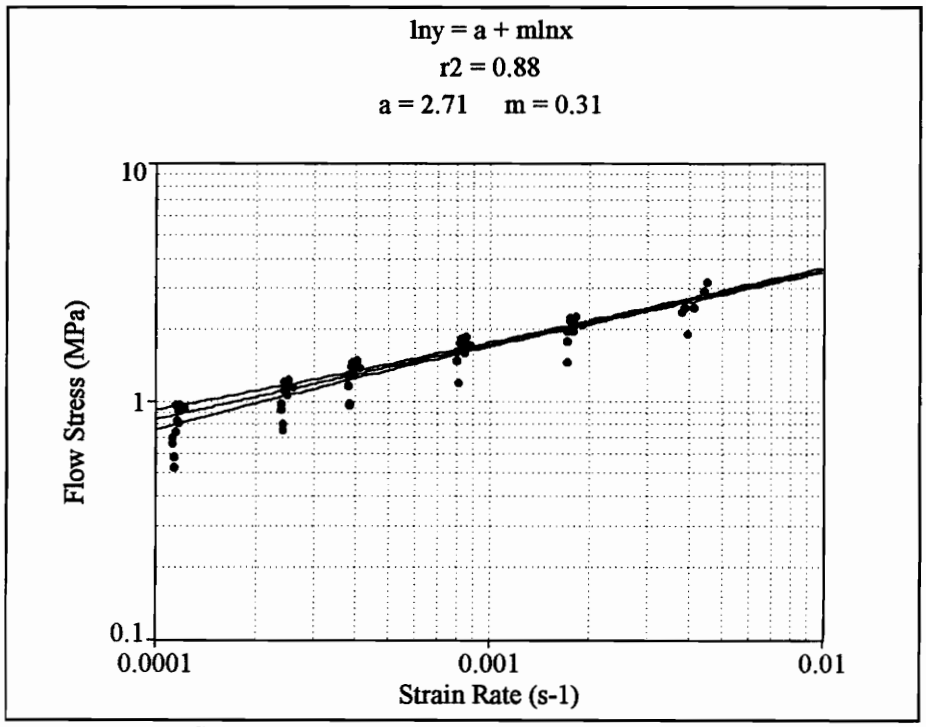

Figure 4.19: Average flow stress vs. strain rate from the compression tests of Bi_2O_3 samples.

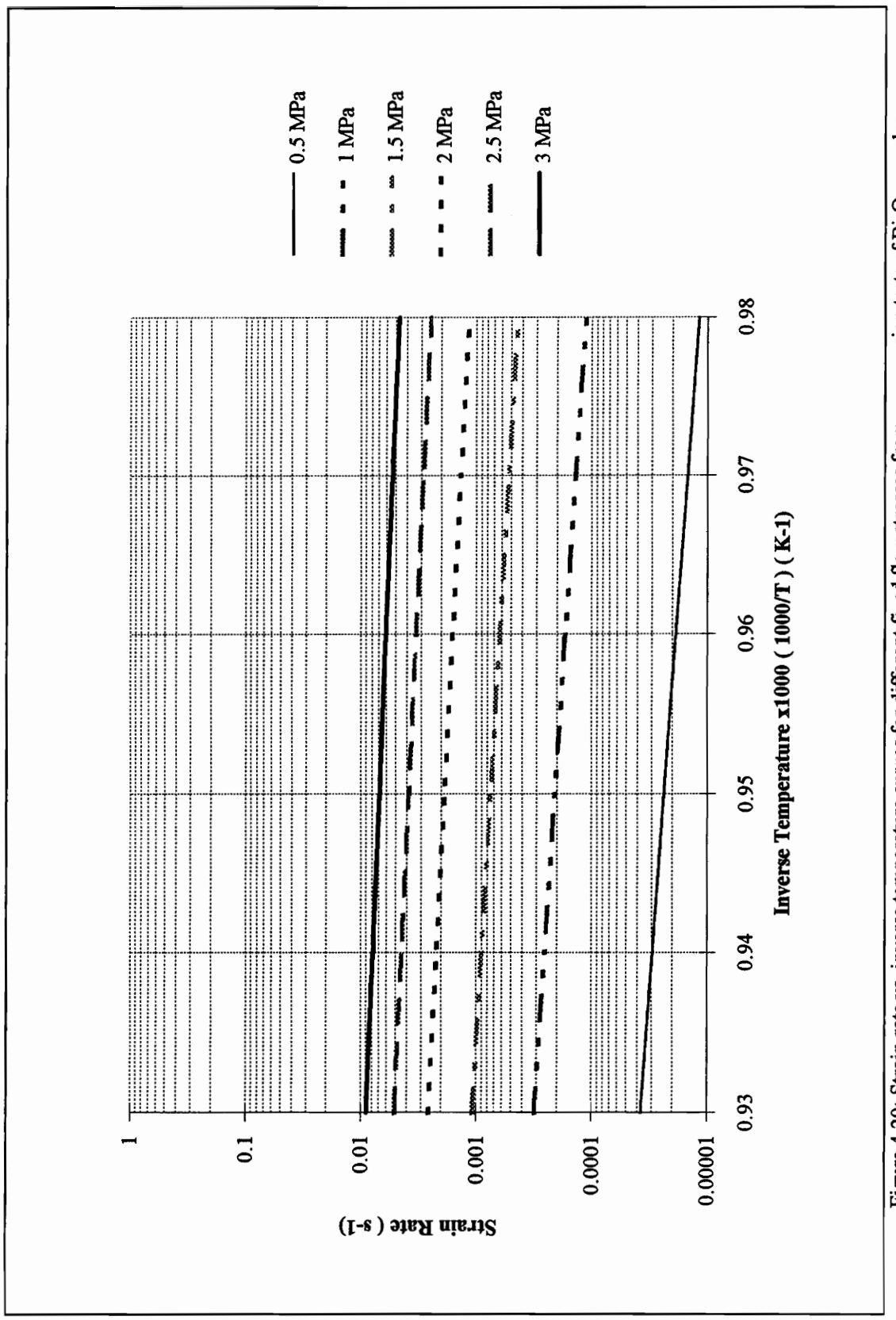

Figure 4.20: Strain rate vs. inverse temperature curves for different fixed flow stresses from compression tests of Bi_2O_3 samples.

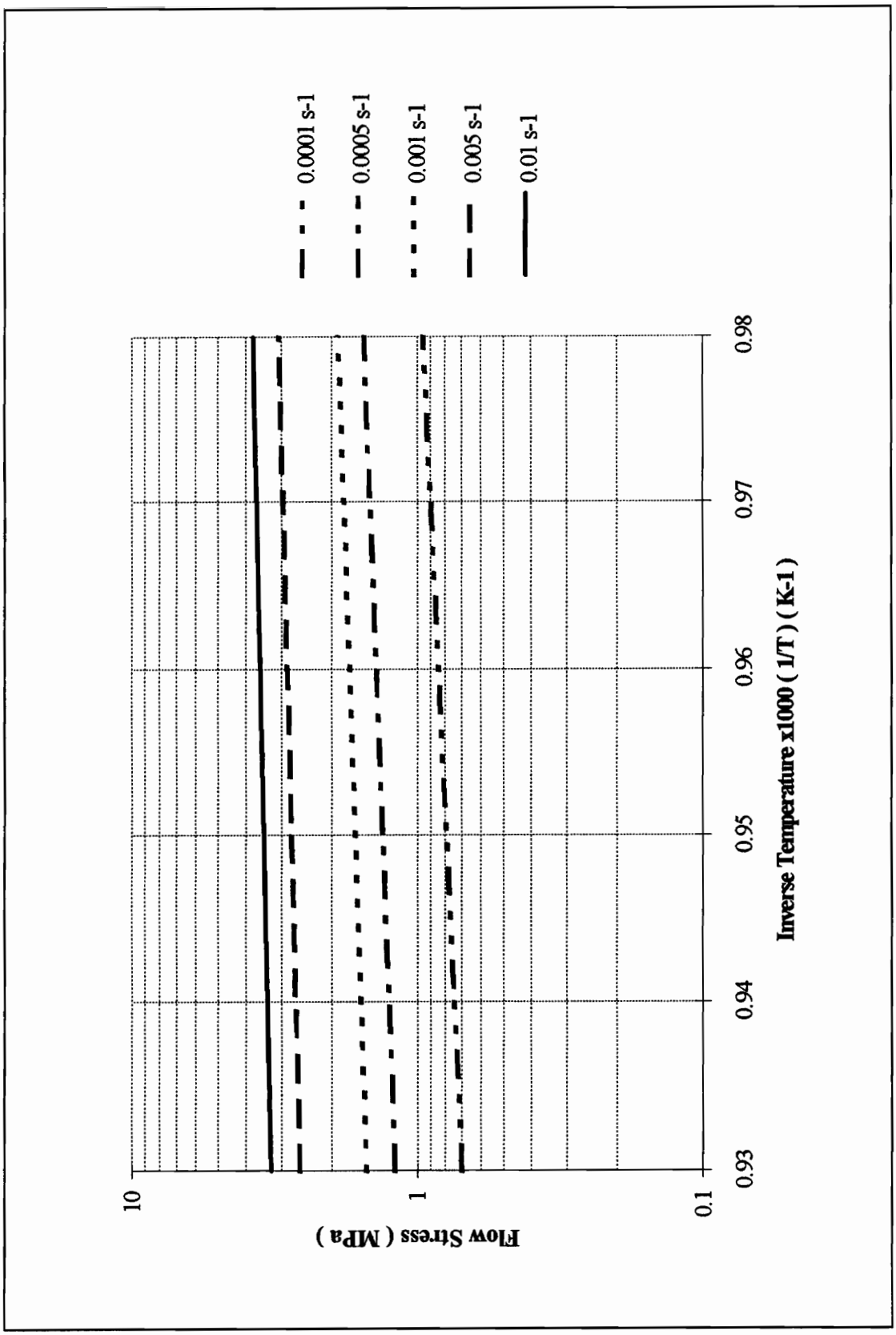

Figure 4.21: Flow stress vs. inverse temperature curves for different fixed strain rates from compression tests of Bi_2O_3 samples.

4.2.3. SUMMARY

Compression tests on samples of bismuth oxides led to the observation of structural superplasticity in the cubic, δ-phase form. No such behavior was observed for the monoclinic phase. The calculated strain-rate sensitivity was a maximum at 775°C, attaining a value of approximatively 0.33. The average activation energy over the temperature range where enhanced plasticity was found to occur was approximately 150 k J/mol.

4.3. RESULTS FOR THE YTTRIA-STABILIZED ZIRCONIA SAMPLES.

4.3.1. TESTS AT ROOM TEMPERATURE.

As previously done for the bismuth oxide, samples of yttria-stabilized zirconia were first tested at room temperature as a reference for later tests at high temperature. The compression tests were performed on five different specimen with the slowest speed achievable, 0.002 mm/s, and resulted in the fracture of each of them after a small displacement of the crosshead as described in Fig. 4.22.

The true stress-true strain curve obtained is characteristic of a ceramic material at room temperature. Indeed, the failure occurred without any plastic deformation at a stress of 33.8 MPa. The Young modulus was derived from the slope of the curve and was estimated to be 1600 MPa.

The fracture surfaces of the samples were then observed with an electronic microscope as illustrated by Fig. 4.23.

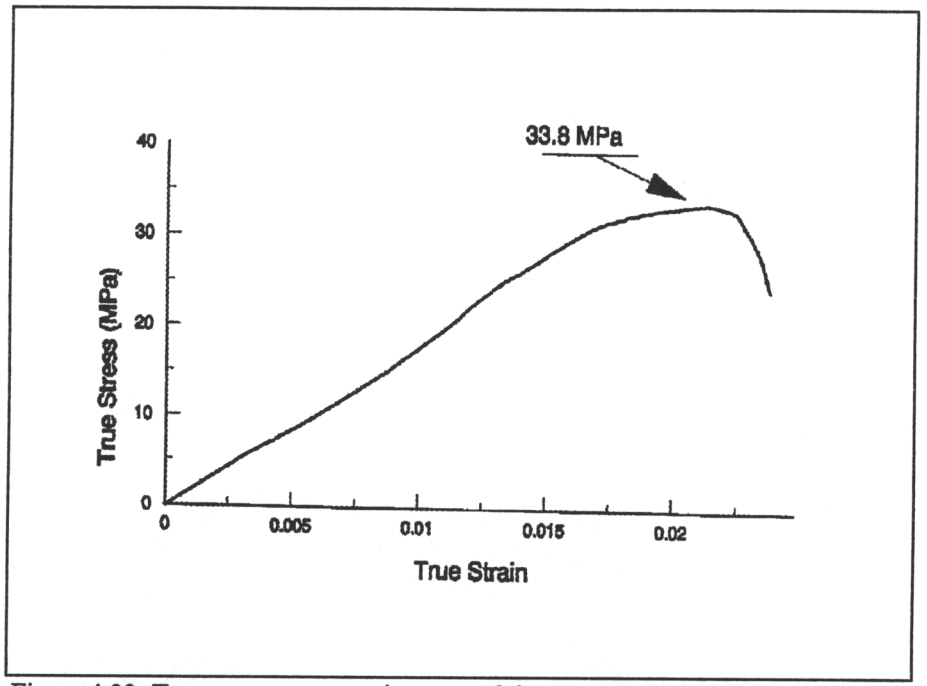

Figure 4.22: True stress - true strain curve of the compression test of a YSZ sample at room temperature with an initial strain-rate of $1.41 \times 10^{-4} s^{-1}$.

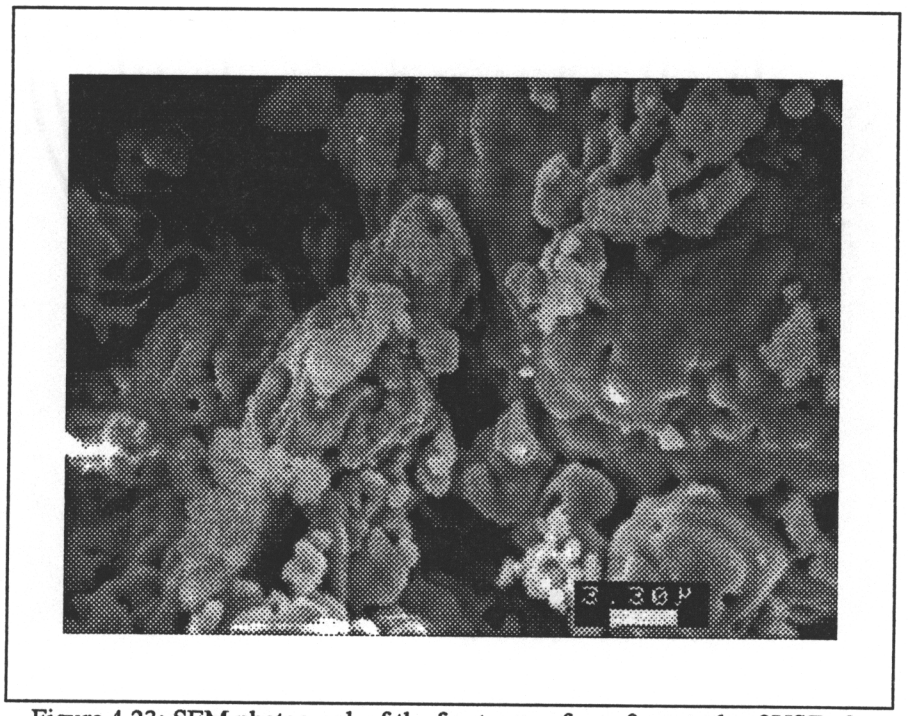

Figure 4.23: SEM photograph of the fracture surface of a sample of YSZ after a compression test at room temperature.

Similar to the case of bismuth oxide, no grains were visible and the surfaces had to be polished and etched. The resulting images, shown in figure 4.24, exhibit grains of various shapes with extensive porosity.

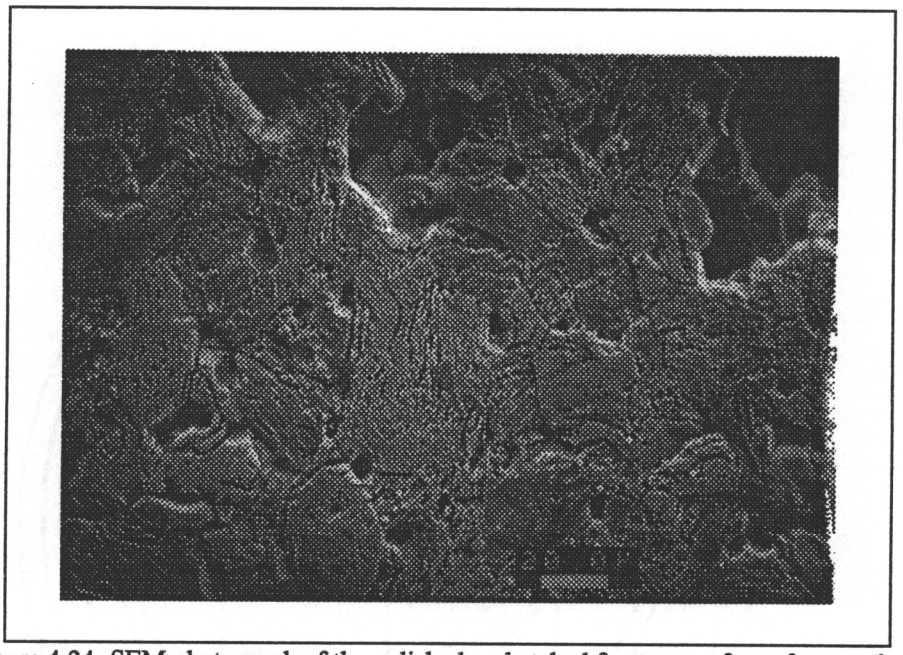

Figure 4.24: SEM photograph of the polished and etched fracture surface of a sample of YSZ after a compression test at room temperature.

4.3.2. TESTS AT HIGH TEMPERATURE.

Whereas tetragonal zirconia has been extensively studied for its structural superplasticity, no exceptional plasticity of cubic zirconia has ever been documented previously in the literature. In the present study, several compression tests, with a crosshead speed of 0.002 mm/s, were performed on YSZ at different temperatures to observe their potential superplastic behavior at temperatures from 1000°C to 1500°C, a range for which the material is reported to be in its cubic phase. The result of these tests are reported in figure 4.25.

Every test resulted in the fracture of the specimen with no plastic deformation, Fig. 4.26.

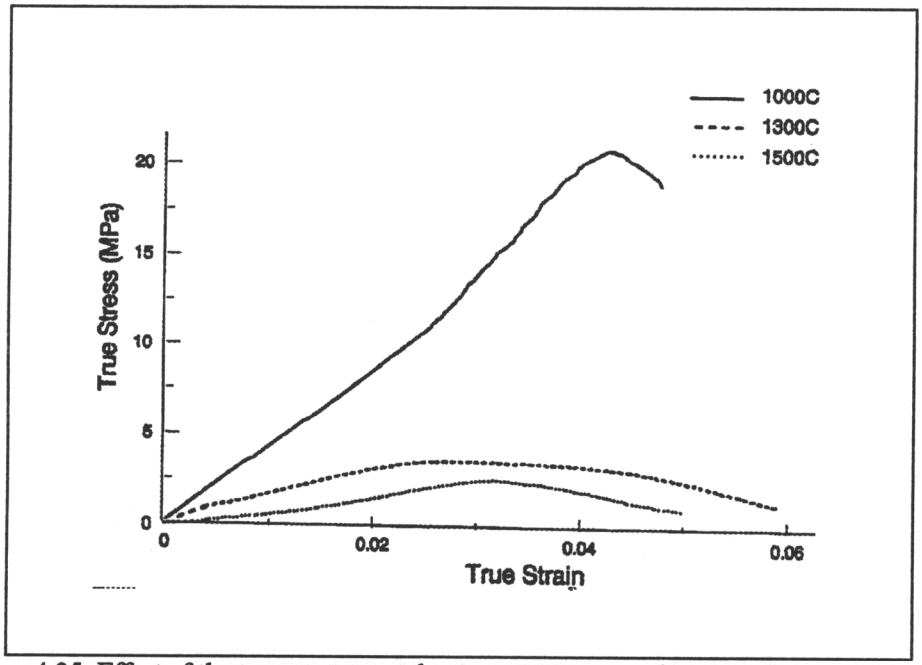

Figure 4.25: Effect of the temperature on the true stress-true strain curve of the compression test of a YSZ sample with an initial strain-rate of $1.06 \times 10^{-4}\ s^{-1}$.

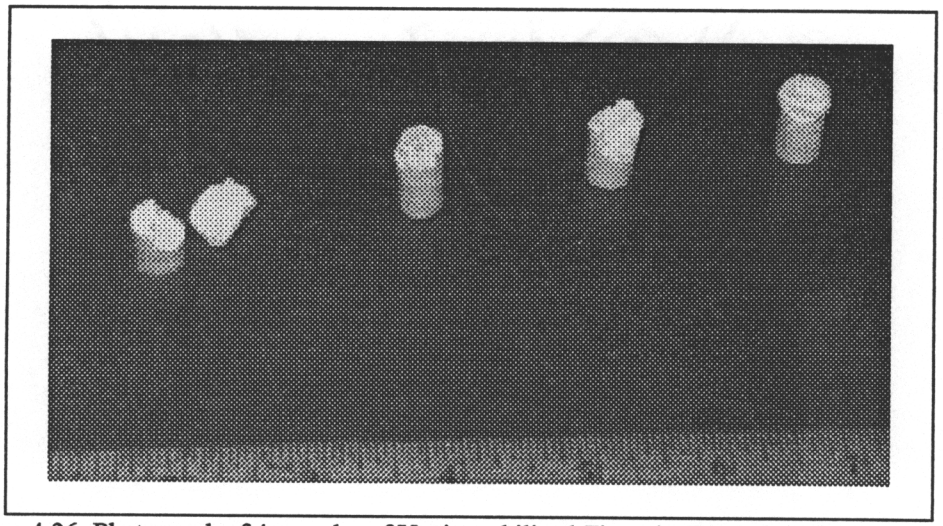

Figure 4.26: Photograph of 4 samples of Yttria-stabilized Zirconia. From the left: Sample after compression test at room temperature, sample after compression test at 1000°C, sample after compression test at 1300°C and sample after compression test at 1500°C.

Nevertheless, the compression strength decreased as the temperature increased. For example, while the stress necessary to break the samples was of 21 MPa at 1000°C, it dropped to 3.6 MPa at 1300°C and to 2.6 at 1500°C. The same tendency was observed with the value of the Young modulus: its initial value at room temperature, 1600 MPa, fell to 490 MPa at 1000°C, to 140 MPa at 1300°C, and to 90 MPa at 1500°C. No tendency for superplasticity was observed. To confirm this observation, compression tests were performed for different crosshead velocities: 0.002 mm/s, 0.006 mm/s and 0.011 mm/s. All the samples tested broke in the same way as before as illustrated by the true stress vs. true strain curves in figure 4.27. The shape of the curves remained characteristic of a brittle material. However as the crosshead speed increased, the compression strength decreased.

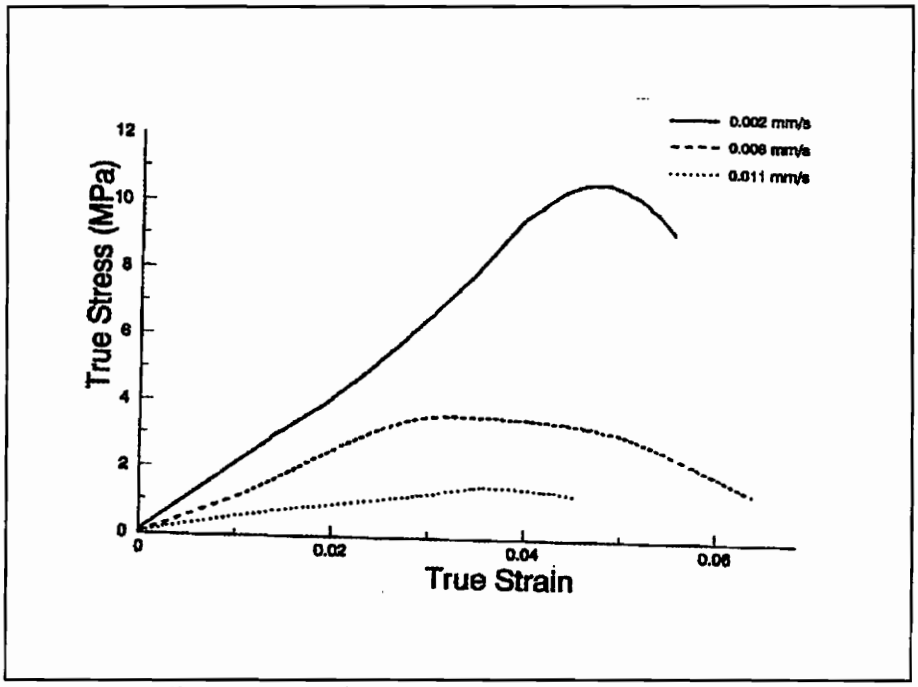

Figure 4.27: Effect of the crosshead speed on the true stress-true strain curve of the compression test of a YSZ sample at 1300°C.

From the performed tests, we were not able to prove any sign of superplasticity in the YSZ samples. Pictures were taken from the fracture surfaces and an example is given in figure 4.28. From these pictures, particles are discernible; hence it is suspected that sintering has not been completed.

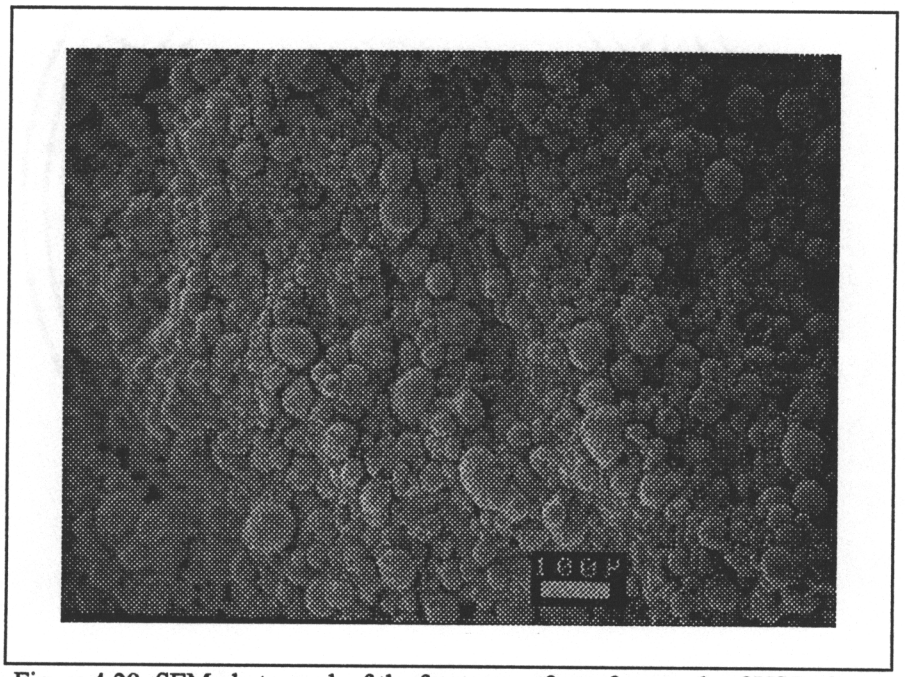

Figure 4.28: SEM photograph of the fracture surface of a sample of YSZ after a compression test at 1300°C.

4.3.3. SUMMARY.

Yttria-stabilized samples were tested in compression for distinct temperatures and neither the monoclinic nor the cubic structure exhibits any tendency to superplastic behavior.

4.4. SUMMARY

- Structural superplasticity was observed in δ-Bi_2O_3 at temperatures in excess of 750°C. Compressive deformations in excess of 85% were observed.

- The strain-rate sensitivity exponent, m, used as a measure of superplasticity, ranged from 0.27 to 0.35 for δ-Bi_2O_3. The maximum value of m occured at 775°C.

- Activation energy associated with the deformation of δ-Bi_2O_3 was calculated to be approximately 150,000 J/mol.

- ZrO2 + 20 wt% Y2O3 (YSZ) exhibited no evidence of superplastic behavior at temperatures ranging from 1000°C to 1500°C.

5. DISCUSSION

5.1. GENERAL CONSIDERATIONS

In the previous chapters, superplasticity and superionic conductivity have both been defined as thermally activated processes. Therefore, it follows that neither of these properties has been observed at room temperature, and that both behaviors have been exhibited by certain ceramic materials where a high diffusion coefficient exists at high temperatures. From this consideration, a possible correlation between these two properties seems conceivable.

On one hand, superplasticity, the ability of a material to exhibit enhanced plasticity, is achieved at high temperature ($T > 0.5$ Tmp) in some materials with small grain size ($d \approx 5$ μm for metals, $d \approx 1$ μm for ceramics) which remains constant during the deformation process. This prerequisite is also a requirement for high diffusivity through the material because of the high density of grain boundaries in the microstructure. Superplastic behavior is generally described in terms of the strain-rate sensitivity, m, and the superplastic activation energy, Q_c, defined by the relation:

$$\dot{\varepsilon} = A \exp(-\frac{Q_c}{RT})(\frac{1}{d})^p \sigma^{1/m} \qquad (2.2)$$

The constants in the above equation are dependent upon the operative the diffusion mechanism. The value of the strain-rate sensitivity varies from 0.2 to 1 in most superplastic materials and provides insight as to the several mechanisms involved. The predominant mechanisms, especially when m is equal to 0.5, are grain boundary sliding

and grain rotation, both accommodated by grain boundary migration. Non-accommodated grain boundary sliding would lead to grain boundary cavitation and thus, to the rupture of the material.

The achievement of superplasticity is strongly influenced by the microstructure. Superplastic materials generally are characterized by fine-grained structures and low porosity. An increase in the grain size or the porosity results in a decrease of the strain rate sensitivity [48]. The same tendency is generally observed in the presence of impurities [27].

On the other hand, superionic conductivity, defined as exceptionally high ionic conductivity, is obtained in some solid materials at high temperature, often after a well-defined phase transformation. This property is also achieved by the motion of ions through the lattice. The movement results in the displacement of charge across the superionic material and, hence, to conduction. As a result, superionic conductivity is directly related to the diffusion coefficient of the charge carrier ions, D(T), by the expression:

$$\sigma(T) = \frac{(Ze)^2}{kT} n(T) D(T). \qquad (2.15)$$

While the influence of the grain size has not been documented in the previous literature, impurities and porosity can also affect the magnitude of the conductivity [49].

It is noted that in an SIC, high ionic mobility is required of only one ionic species. Hence, in the presence of an electric field, a gradient in composition develops. The composition gradient is present despite an opposing tendency to maintain charge neutrality in all locations of the ionic material.

During high temperature deformation of ceramics, however, it is generally assumed that mass transport of all ionic species must simultaneously occur to maintain stoichiometric and charge neutrality constraints. A correlation of superionic conductivity to superplastic deformation would necessitate the speculative assumption that atomic diffusion of one atomic species can dominate the material's effort to maintain volumetric continuity, i.e., that a transient compositional gradient can be established in response to a strain.

5.2. CONSIDERATIONS ON BISMUTH OXIDE

Samples of bismuth oxide were prepared in the form of ∅10x15 mm cylinders through cold pressing followed by sintering. The fabricated samples, with a grain size of 9 μm and a relative density of 86%, were tested in compression. Enhanced plasticity is observed in the δ-Bi_2O_3 with deformation up to 85%, attaining steady-state flow with no fracture (Figs. 4.6, 4.7) at temperatures in excess of 750°C. Further, velocity jump tests were performed in the same range of temperatures and led to a maximum value of m of 0.33 at 775°C and to a value of the activation energy 150±30 kJ/mol.

Several conclusions can be drawn from these results and observations.

The flow stress vs. strain-rate curves are characteristic of superplastic ceramics [14]. Only one slope is discernible at each temperature, corresponding to a strain-rate sensitivity ($m \approx 0.3$) in the range of superplastic behavior of ceramic materials. Nevertheless, the initial microstructure was not ideal. More specifically, the grain size of 9 μm was about five times larger than that observed in the superplastic ceramics documented in the literature [13,14,18-20,23-30]. Similarly, the relative density (86%) was low compared to the 95-98% found in the previously reported superplastic materials. As a consequence, we can suppose that Bi_2O_3 samples with a higher density and a smaller grain size would be even more likely to exhibit superplasticity and, possibly, lead to a higher value of m.

Further evidence that the values of m obtained in the present work may be uncharacteristically low for this material is provided by the post-deformation microscopy (Fig. 4.9). As noted, two distinct microstructures are observed; the first consisting of equiaxed grains and the second of highly deformed, elongated grains. True superplasticity leads to little or no grain-shape changes. While this was confirmed in certain areas of the deformed microstructures, obvious evidence of gross shape changes was also present. As a result, the experimentally-derived values of m in the present work may actually represent an average of that characteristic of the equiaxed regions (higher m presumed) and that of the deformed regions (lower m expected). Following this logic, it is conceivable that the optimum microstructure and conditions leading to superplasticity were not attained in the present work.

The observed temperature dependence of the strain-rate sensitivity (Fig. 4.18) may also be the result of microstructure considerations. Whereas the lowest value calculated from the data acquired at 750°C may be the result of an insufficient thermal activation, the low value found at 800°C can be caused by grain growth activated by the increase in temperature.

It is also possible that porosity can exert an influence on the measured strain-rate sensitivity. The origin of an effect, however, would be related to the magnitude of the flow stress of the material. For example, the relationship relating the flow stress and the strain-rate to the strain-rate exponent m, i.e.,

$$m = \frac{\delta \ln \sigma}{\delta \ln \dot{\varepsilon}} \qquad (2.1)$$

can also be expressed as

$$m = \frac{\dot{\varepsilon}}{\sigma} \cdot \frac{\delta \sigma}{\delta \dot{\varepsilon}}. \qquad (5.1)$$

It follows that porosity in the sample under compressive loading conditions may lead to an inaccurately low value of flow stress and result in a slightly larger value of m for the actual volume of material undergoing deformation. Nonetheless, the magnitude of such an effect on m for the differences in flow stress attributable to porosity are insignificant and outside the resolution of the values of m reported. It is further noted that, in the absence of fracture, porosity is not expected to directly affect the inherent strain-rate sensitivity or deformability of the material.

Finally, the variation of the strain-rate sensitivity with temperature results in an element of uncertainty in the calculation of the activation energy of the deformation. The value of this constant may also be sensitive to the microstructure and to the mechanistic details governing deformation. It is further noted that since structural superplasticity has never been documented before, no data is available in the literature for comparison.

The activation energy for superionic conductivity of pure cubic bismuth oxide has been reported to be equal to 39 kJ/mol by Harwig and Gerards [37]. This value is about four times lower than the energy calculated in the present study governing the deformation process. Since the mechanistic role of the activation energy for both ionic conductivity and superplasticity is diffusional in origin, one would expect that these values would be comparable. That they do vary by a factor of four does not necessarily eliminate the correlation ultimately sought, however. For example, the microstructural details (e.g., grain size, presence of impurities, etc.) associated with the material used by Harwig was not reported; hence, its extension to the material of the present work is of questionable value. Secondly, as noted above, uncertainties with respect to the calculated value of Qc in the present study attributable to the microstructure inhomogeneities are also present. In this regard, one might expect that a microstructure more fully capable of

superplasticity may lead to a lower value of Q_c (e.g., smaller grain size might lead to the dominance of a smaller activation energy characteristic of grain boundary processes). Further, other incompatibilities, such as differences in processing techniques employed, presumably would also lead to differences in the thermal response of conductivity and deformation.

As a result of these considerations, two alternative future trends can be recommended.

First, ionic conductivity measurements should be effected on identically-processed Bi_2O_3 samples to facilitate direct comparison of the activation energies of both phenomena. The measurements can be done by impedance analysis [48] or by measuring the electrical conductivity and the e.m.f. of an oxygen concentration cell [49].

Secondly, superplasticity of cubic bismuth oxide requires more investigation, especially on samples of higher density and over a range of grain sizes. By this way, the superplastic activation energy and strain-rate response could be more thoroughly analyzed.

5.3. CONSIDERATIONS ON YTTRIA-STABILIZED ZIRCONIA

The same experimental procedure was followed for the processing of the yttria-stabilized zirconia samples. The YSZ powder was pressed in ∅10x15 mm cylinders and sintered. The grain size of the specimen was 27 μm and the relative density was 66%.

Compression tests were performed at different temperatures between 1000°C and 1500°C and no plasticity was detected. This behavior was predictable since the initial microstructure did not fulfill the superplasticity requirements which were small grain size and high density.

Future efforts for this material would be to modify the processing parameters so that the sample exhibit a "superplastic microstructure". This could be achieved by increasing the pressure during cold pressing and by increasing the sintering temperature to 1800 or 2000°C [50]. When a grain size in the magnitude of 1 μm and a density close to 98% would be achieved, the procedure tests applied earlier to the bismuth oxide samples should be used. If superplastic deformations are exhibited, conductivity measurements on the same type of samples should be made and activation energies should be compared.

The percentage of yttria could also be varied from 3 mol% to 12 mol%. Two compositions would be particularly interesting to study: the 3 mol% yttria-stabilized tetragonal zirconia since it is documented for its superplastic behavior but not for its superionic conductivity [13,14,18-20,25-30], and the 8 mol% yttria-stabilized zirconia which corresponds to the YSZ exhibiting the highest ionic conductivity [44].

6. CONCLUSION

- Structural superplasticity was observed in δ-Bi_2O_3 at temperatures in excess of 750°C. Prior to this investigation, only transformational superplasticity has been documented in the literature.

- Correlations between superplasticity behavior and superionic conductivity remain inconclusive. Results which support this potential conclusion include the observation that superplasticity in Bi_2O_3 can occur over the temperature range where ionic conductivity is reported to occur. Prior investigations have reported only transformation superplasticity for Bi_2O_3; this would be incompatible with any correlation.

  Results which do not support the correlation include a factor-of-four difference in the experimentally-determined activation energy for deformation from the reported activation energy for superionic conductivity in this material. However, uncertainties exist as to whether these values can be legitimally compared.

- The YSZ exhibited no evidence of superplastic deformation. however, the microstructure of the samples was not representative of that required for superplastic deformation of this material.

REFERENCES

1. N.E. Paton and C.H. Hamilton, in *Superplastic Forming of Structural Alloys* (conf. proc.), TMS-AIME, (1982).
2. J. Pilling and N. Ridley, in *Superplasticity in crystalline solids*, edited by the Institute of Metals, (1989), pp. 1-39.
3. M.G. Lozinsky and I.S. Simeonova, "Super high plasticity of commercial iron under cyclic fluctuations of temperatures", *Acta. Met.*, 7, 709-715, (1959).
4. A. Sauveur, "What is steel? - Another answer.", *Iron Age*, 113, 581-583, (1924).
5.* F. Koref, *Z. Technm. Physik*, 7,544, (1926).
6. M. de Jong and G.W. Ratheneau, "Mechanical properties of iron and some iron alloys while undergoing allotropic transformation", *Acta. Met.*, 7, 246-253, (1959).
7. C.A. Johnson, R.C. Bradt and J.H. Hoke, "Transformational plasticity in Bi_2O_3", *J. Amer. Ceram. Soc.*, 58, 37-40, (1975).
8. G.D. Bengough, "A study of the properties of alloys at high temperatures", *J. Inst. Met.*, 7, 123, (1912).
9. O.D. Sherby and J. Wadsworth, "Observations on historical and contemporary developments in superplasticity", in *Superplasticity in metals, ceramics and intermetallics*, edited by M.J. Mayo, M. Kobayashi and J. Wadsworth, (MRS, Pittsburg, PA, 1990), pp. 3-14.
10. C.E. Pearson, "The viscous properties of extruded eutectic alloys of lead-tin and bismuth-tin", *J. Inst. Met.*, 54, 111, (1934).
11. E.E. Underwood, "A review of superplasticity and related phenomena", *Jour. Metals*, 14, 914-919, (1962).
12.* W.A. Backofen, I.R. Turner and D.H. Avery, *Trans. ASM*, 57, 980-990, (1964).
13. F Wakai, S. Sakagushi and Y. Matsuno, "Superplasticity of Yttria-Stabilized Tetragonal ZrO_2 Polycrystals", *Adv. Ceram. Mater.*, 1, 259-263, (1986).
14. Y. Maehara and T.G. Langdon, "Review: Superplasticity in ceramics", *J. Mater. Sci.*, 25, 2275-2286, (1990).
15. L.F. Porter and P.C. Rosenthal, "Effect of applied tensile stress on phase transformations in steel", *Acta. Met.*, 7, 504-514, (1959).
16. F.W. Clinard and O.D. Sherby, "Strength of iron during allotropic transformation", *Acta. Met.*, 12, 911-919, (1964).
17. G.W. Greenwood and R.H. Johnson. "Deformation of metals under small stresses during phase transformations", *Proc. Roy. Soc. Sr. A*, 283, 403-442, (1965).
18. T.G. Nieh, C.M. McNally and J. Wadsworth, "Superplasticity in intermetallic alloys and ceramics", *J. O. M.*, 42, 31-35, (1989).
19. T.G. Nieh and J. Wadsworth, "Superplastic ceramics", *Ann. Rev. Mater. Sci.*, 20, 117-140, (1990).
20. T.G. Langdon, "Superplastic ceramics: They're not a stretch of the imagination anymore.", *J.O.M.*, 8-13, (1990).

21. J.L. Hart and A.C.D. Chaklader, "Superplasticity in pure ZrO_2", *Mat. Res. Bull.*, 2, 521-526, (1967).
22. J.R. Smyth, R.C Bradt and J.H.Hoke, "Transformational superplasticity in the Bi_2O_3-Sm_2O_3 eutectoid system", *J. Amer. Ceram. Soc.*, 58, 381-384, (1975).
23. P.C. Panda, R. Raj and P.E.D. Morgan, "Superplastic deformation mechanisms in a fine-grained $MgO\text{-}2Al_2O_3$ spinel", *J. Amer. ceram. Soc.*, 68, 522-529, (1985).
24. F. Wakai, Y. Kodama, S. Sakagushi, N. Murayama, K. Izaki and K. Niihara, "Superplasticity of non-oxide ceramics", in *Superplasticity in metals, ceramics and intermetallics*, edited by M.J. Mayo, M. Kobayashi and J. Wadsworth, (MRS, Pittsburg, PA, 1990), pp. 349-358.
25. T.G. Nieh and J. Wadsworth, "Superplastic deformation in a fine-grained Yttria-stabilized Tetragonal Zirconia Polycrystal (Y-TZP)", in *Superplasticity in metals, ceramics and intermetallics*, edited by M.J. Mayo, M. Kobayashi and J. Wadsworth, (MRS, Pittsburg, PA, 1990), pp. 331-336.
26. T. Nagano, H. Kato and F. Wakai, "Superplasticity in mullite-zirconia composite", *J. Mater. Sci.*, 27, 3575-3580, (1992).
27. C. Carry, "Microstructures, grain boundaries and superplasticity in fine-grained ceramics", in *Superplasticity in metals, ceramics and intermetallics*, edited by M.J. Mayo, M. Kobayashi and J. Wadsworth, (MRS, Pittsburg, PA, 1990), pp. 313-323.
28. Y. Ma and T.G. Langdon, "An investigation on the mechanical behavior of a superplastic Yttria-stabilized Zirconia", in *Superplasticity in metals, ceramics and intermetallics*, edited by M.J. Mayo, M. Kobayashi and J. Wadsworth, (MRS, Pittsburg, PA, 1990), pp. 325-330.
29. T.G. Nieh, C.M. Tomasello and J. Wadsworth, "Dynamic grain growth in superplastic Y-TZP and Al_2O_3 / YTZ", in *Superplasticity in metals, ceramics and intermetallics*, edited by M.J. Mayo, M. Kobayashi and J. Wadsworth, (MRS, Pittsburg, PA, 1990), pp. 343-348.
30. A.H. Chokshi, D.J. Schissler, T.G. Nieh and J. Wadsworth, "A comparative study of superplastic deformation and cavitation failure in a Yttria-Stabilized Zirconia and a Zirconia-Alumina composite", in *Superplasticity in metals, ceramics and intermetallics*, edited by M.J. Mayo, M. Kobayashi and J. Wadsworth, (MRS, Pittsburg, PA, 1990), pp. 379-384.
31. J.B. Boyce and B.A. Huberman, "Superionic conductors: Transitions, structures, dynamics", *Physics Reports*, 51, 189-265, (1979).
32. L.L. Hench and J.K. West, in *Principles of electronic ceramics*, edited by Wiley-Interscience Publication, (1990), pp 136-163.
33. H.L. Tuller and P.K. Moon, "Fast ion conductors: future trends", *Mater. Sci. and Eng.*, B1,171-191, (1988).
34. H. Yugami and M. Ishigame, "Fundamental physics and promising applications of superionic conductors", *Jpn. J. Appl. Phys.*, 32, 853-859, (1993).
35. E.M. Levin and R.S. Roth, "Polymorphism of Bismuth Sesquioxide. I. Pure Bi_2O_3", *J. Res. Nat. Bur. Std.*, 68A, 189-195, (1964).

36. M.J. Verkerk and A.J. Burggraaf, "High Oxygen Ion Conduction in Sintered Oxides of the Bi_2O_3-Dy_2O_3 System", *J. Electrochem. Soc.*, 128, 75-82, (1981).
37. H.A Harwig and A.G. Gerards, "Electrical properties of the α, β, γ, and δ phases of bismuth sesquioxide", *J. Solid State Chem.*, 26, 265-274, (1978).
38. P. Su and V. Virkar, "Ionic conductivity and phase transformation in Gd_2O_3-stabilized Bi_2O_3", *J. Electrochem. Soc.*, 139, 1671-1676, (1992).
39. M.J. Verkerk, K. Keizer and A.J. Burggraaf, "High oxygen ion conduction in sintered oxides of Bi_2O_3-Er_2O_3 system", *J. Appl. Electrochem.*, 10, 81-90, (1980).
40. T. Takahashi, H. Iwahara and Y. Nagai, "High oxide ion conduction in sintered Bi_2O_3 containing SrO, CaO or La_2O_3", *J. Appl. Electrochem.*, 2, 97-104, (1972).
41. T. Takahashi and H. Iwahara, "High oxide ion conduction in sintered oxides of the system Bi_2O_3-WO_3 ", *J. Appl. Electrochem.*, 3, 65-72, (1973).
42. E.C. Subbarao, "Zirconia - an overview", in *Science and technology of zirconia*, edited by A.H. Heuer and L.W. Hobbs, (The American ceramic society, Inc., Columbus, OH, 1981), pp.1-24.
43. D.W. Strickler and W.G. Carlson, "Electrical conductivity in the ZrO_2-rich region of several M_2O_3-ZrO_2 systems", *J. Amer. Ceram. Soc.*, 48, 286-289, (1965).
44. J.M. Dixon, L.D. LaGrange, U. Merten, C.F. Miller and J.T. Porter, "Electrical resistivity of stabilized zirconia at elevated temperatures", *J. Electrochem. Soc.*, 110, 276-280, (1963).
45. V.S. Stubican, R.C. Hink and S.P. Ray, "Phase equilibria and ordering in the system ZrO_2-Y_2O_3 ", *J. Amer. Ceram. Soc.*, 61, 17-21, (1978).
46. J.S Reed, in *Introduction to the principles of ceramic processing*, edited by Wiley-Interscience Publication, (1988).
47. W.D. Kingery, H.K. Bowen and D.R. Uhlmann, in *Introduction to ceramics, second edition*, edited by Wiley-Interscience Publication, (1976).
48. R. Duclos, J. Crampon and B. Amana, "Structural and topological study of superplasticity in zirconia polycrystals", *Acta metall.*, 37, 877-883, (1989).
49. T.A. Ramanarayanan, "Limiting factors in measurements", in *Solid electrolytes and their applications*, edited by E.C. Subbarao (Plenum press, New York, NY, 1980), pp. 81-98.
50. D.W. Strickler and W.G. Carlson ," Ionic conductivity of cubic solid solutions in the system CaO-Y_2O_3-ZrO_2", *J. Amer. Ceram. Soc.*, 47, 122-127, (1964).

---

* Cross reference

VITA

The author was born on September 22, 1971, in Quessy-Centre, France. She spent her childhood in Tergnier, a lovely small town in Picardie, one of the rainiest parts of France. Upon completing high school, she pursued her studies at the "Université de Technologie de Compiègne", U.T.C., France, in the department of Engineering Mechanics. While studying at the U.T.C., she participated in the U.T.C.-Virginia Tech. exchange program to enroll in the Master Program in Materials Science and Engineering at V.P.I.&S.U. in August 1992. She recieved her French "Diplôme d'ingénieur" in June 1994.